Physics – Uspekhi **45** (4) 369 – 402 (2002)

REVIEWS OF TOPICAL PROBLEMS

PACS numbers: **73.22. – f**, 73.63.Fg, 81.07.De

Carbon nanotubes and their emission properties

A V Eletskiĭ

DOI: 10.1070/PU2002v045n04ABEH001033

Contents

Abstract. The current methods of synthesis and investigation of carbon nanotubes are reviewed. The interconnection between structural peculiarities and electronic characteristics of carbon nanotubes has been studied. The recently developed methods of growth of similar nanotubes with pre-assigned characteristics are described. The development of these methods offers the possibility of mass production and application of relevant devices. The phenomenon of electron field emission from carbon nanotubes and possibilities of its usage in flat panel displays, gas discharge devices, etc. is analyzed. Prospects and real achievements in the area of application of nanotubes as cold electron emission sources are discussed.

1. Introduction

A nanotube is an elongated fullerene. The end of the 20th century was noted with the discovery of new modifications of carbon, which are closed surface structures consisting of hexagons and pentagons with carbon atoms at their vertices. Fullerenes and carbon nanotubes are the most interesting versions of these new carbon structures. The surface of fullerenes has a closed spherical or spheroidal form [1 – 3]. The surface structure of fullerenes contains not only regular hexagons, whose number depends on the fullerene size, but also 12 pentagons arranged in a regular manner over the surface. The discovery of fullerenes was awarded with the Nobel Prize for Chemistry in 1996 [4 – 6].

More than 10 years have passed since the discovery of carbon nanotubes (CNT) [7]. These are elongated cylindrical structures ranging from one to several tens of nanometers in diameter and up to several micrometers in length, consisting of one or several hexagonal graphitic layers rolled into a tube. A nanotube is ended usually with a hemispherical cap which can be considered as half of a fullerene molecule.

Nanotubes were first discovered in soot formed in the conditions of an arc discharge with graphite electrodes. Such a discharge is used effectively, in particular, for large-scale production of fullerenes [2].

As was noted wittily by W Kratschmer, shortly after their discovery nanotubes were considered as elongated fullerenes. Nevertheless, further studies have shown that the class of carbon nanotubes in the variety of their structures and physical and chemical characteristics exceeds considerably that of fullerenes. For this reason it seems to be more proper to consider a fullerene molecule as a limiting case of a carbon nanotube, the two caps of which are joined directly with each other. However, as distinct from fullerenes which are a molecular modification of carbon, CNTs combine the properties of both molecules and the solid state and can be considered as an intermediate state of the substance (between molecular and condensed ones). This peculiarity attracts the continuously rising interest of researchers addressed to the exploration of fundamental peculiarities in the behavior of such an exotic object in various conditions.

In the last few years one could observe a real boom of investigations directed to production, establishing physical and chemical properties and determining ways for the most effective practical application of CNTs. Thousands of papers are published on this subject every year. These investigations have resulted in a quick change in our notion about the mechanisms of synthesis of CNTs in various experimental conditions, about their structural features and physical and chemical behavior, and also about possible applications. For this reason the author's review article devoted to carbon nanotubes [8], published in *Physics-Uspekhi* about 5 years ago, has become rather antiquated and now is of only historical interest.

Considerable progress in the investigation of fundamental physical and chemical properties of CNTs, in the development of new effective methods for their produc-

A V Eletskiĭ. Russian Research Centre 'Kurchatov Institute', pl. Kurchatova 1, 123182 Moscow, Russian Federation
Tel./Fax (7-095) 196 72 80
E-mail: eletskii@imp.kiae.ru

Received 26 June 2001
Uspekhi Fizicheskikh Nauk **172** (4) 401 – 438 (2002)
Translated by A V Eletskiĭ; edited by A Radzig

tion, and also in elaboration of ways for practical use of these unique objects has been made during the 5 years after the publication of the cited review article. Thus, the transition of a CNT-containing material into a superconducting state was reported recently [9, 10]. Mechanisms of conductivity peculiar to CNTs of various structures in different physical conditions have been studied in detail. An interconnection between Raman spectra of single-walled CNTs and their diameter has been stated [11].

This article contains a review of a circle of problems related to the emission characteristics of CNTs. Structural features of CNTs and their interconnections with electrical properties and emission characteristics are analyzed. Methods for production and investigation of CNTs have been discussed. Here special attention is paid to methods providing the formation on a large area of well-aligned layers of CNTs with close structural and electronic characteristics. The behavior of CNTs under the action of an external electric field and, in particular, mechanisms of the electron field emission are reviewed and analyzed. The first CNT-based flat panels and cathode ray lighting tubes are also described. Most attention is concentrated on data obtained between 1998 and 2000, which have not yet been reflected in reviews and monographs.

The applied value of CNTs. As follows from investigation results, there is a great variety of conditions where the effective formation of CNTs is observed. Thus, nanotubes were produced not only in arc discharge but also through the thermal sputtering of a graphite surface in an inert gas atmosphere with a laser [12] and even with focused solar irradiation [13]. One more effective approach to the synthesis of CNTs is based on chemical processes proceeding during the high-temperature interaction of hydrocarbons with metal catalysts. This set of processes includes the thermocatalytic decomposition of hydrocarbons [14], chemical vapor deposition from plasma containing hydrocarbons [15], etc. Among other approaches to production of the CNT one can mention, in particular, the electrolytical method based on passing an electric current through graphite electrodes immersed in a liquid electrolyte [16]; a method based on a chemical transformation of a solid polymer into a CNT-containing material [17]; pyrolysis of solid-state refractory carbon compounds [18], and direct catalytic transformation of composite powders [19]. As was recently found, CNTs form effectively in flames as a result of burning hydrocarbons [20].

The physical and chemical properties of CNTs and relevant applied issues are now studied in tens of laboratories all over the world. A series of monographs and review articles has been published (e.g., see Refs [21 – 23]), where the results of basic and applied research in the field are presented. Several international conferences are held annually, where the results of recent research and development related to carbon nanotubes are considered. The interest in this topic is caused, on the one hand, by the extraordinary physical and chemical properties of CNTs making them an attractive subject of basic research and, on the other hand, by promising prospects of practical use of such objects. Among the most interesting properties of CNTs one should first mention the interconnection between the geometrical structure and electronic characteristics of these carbon compounds [8, 21 – 23]. A nanotube can possess either metallic conductivity or semiconducting properties, depending on the orientation angle of the graphite layer, constituting the nanotube in relation to its axis (chirality). In this case such an important characteristic of electronic properties of a semiconducting nanotube as its energy gap width is determined by its geometrical parameters, which are the angle of chirality and diameter. Carbon nanotubes represent in essence a new class of electronic devices of extraordinary small size. Development of integrated circuits involving CNT-based elements could result in drastical change in the field of miniaturization of modern computers.

The second important basic property of CNTs relates to their high aspect ratio, due to which the electric field strength in the vicinity of the nanotube's cap is hundreds times higher than the relevant volumetrically averaged magnitude of that generated by an external source. This in its turn results in an extraordinarily high value of the electron emission current at a relatively low applied voltage [24, 25]. Therefore, the electron field emitters with CNT-containing cathodes are beyond comparison with other field emission devices. Flat panel displays and cathode ray lighting tubes [26] fall in this category. By this means the development of CNT-based emitters results in the creation of a new class of electronic devices distinguished by their extraordinary small lateral sizes and low magnitude of power voltage.

One more important property of CNTs relates to the possibility of their filling with gaseous or liquid substances [27]. Since the CNT is a purely surface structure, its mass is contained exclusively in the surface of its layers. This culminates in the anomalously high specific surface of nanotubes, which in turn is reflected in their electrochemical and sorption characteristics. The distance between graphitic layers in a multilayer carbon nanotube is close to that for crystal graphite (3.4 nm). This distance is quite large so that some amount of a substance can be housed inside a CNT. By this means a CNT can be considered as a unique container for storage of a substance in gaseous, liquid or solid state. If this substance can be sorbed on the inner surface of the graphitic layer comprising the nanotube, the density of the sorbed substance can reach that of the condensed state.

A substance penetrates inside a nanotube under the action of an external pressure or as a result of the capillary effect and is kept in the interior due to sorption forces. In this case the graphite shell protects the enclosed substance from external chemical or mechanical action quite well. Therefore, CNTs can be considered as a potential means for storage of a substance over extended periods. In particular, gaseous hydrogen storage devices on the basis of CNTs comprise the subject of current intensive research and development [28]. One can expect that the success with these efforts will result in the creation of a new type of car engine fuelled by hydrogen and distinguished by a high degree of environmental safety.

Mechanical properties of CNTs are also quite attractive in relation to possible applications. Nanotubes possess an extraordinary high tensile and bending strength [29]. This allows their use just now as an active element of measuring devices in determining the nanometer-sized structure of surfaces [30]. Inserting even a small quantity of CNTs into composite polymer materials considerably improves their mechanical properties [31]. An interconnection between the mechanical load applied to a CNT and its electrical properties [32] has been found recently. This opens up a new field of research involving nanometer-sized optoacoustic phenomena. The research may result in the development and design of superminiature transformers of

a mechanical signal into an electric one (and the opposite). Eventually this may change the current status of acoustic devices and such fine instruments for studying surface structure as the atomic field microscope.

As is seen, the range of possible scientific and technological applications of CNTs is exceptionally wide. The list of such applications can easily be enlarged. This article concerns one of the most advanced directions related to the investigation and employment of CNTs as a source of electron field emission. The quick development of this direction has resulted in the creation of competitive flat panel displays distinguished by a low voltage, a low power supply, and also a high degree of spatial and time stability of emission characteristics.

Already the first reports about observation and study of the field emission in CNTs [24, 25] showed an attractive possibility of using these objects as effective sources of electron field emission. Two main features of CNTs determine this possibility, namely, their high aspect ratio and good electrical conductivity. Due to these features, a quite high electron field emission current (at the level of 1 mA cm^{-2}) is observable for CNT-containing cathodes at a relatively low magnitude of applied voltage ($\sim$ 1000 V at an interelectrode gap of a fraction of a millimeter). The development of the methods for growing 2D matrices of well-aligned CNTs on a large area of a specially prepared surface of a substrate [33, 34] has become an important stage on the way to the practical realization of the above-mentioned advantages of CNT-based electron field emitters. This permits one to impart the character of large-scale production to the procedure of fabrication of large microschemes, including CNT-based field emission cathodes, using well-developed methods of chemical deposition in combination with photolithography. A practical realization of these methods has resulted in creating competitive flat panel displays and cathode ray lighting sources with CNT-based cathodes, possessing high operative characteristics. Therefore one can conclude that researchers have passed in a comparatively short space of time (about 10 years) a long way from the discovery of carbon nanotubes to creating effective competitive electronic devices operating on their basis. This is in essence the first direction of applied usage of CNTs, which is close to a practical realization in industry.

2. The structure of nanotubes

2.1 Single-walled nanotubes

Chirality. An ideal nanotube is a graphite plane rolled into a cylinder, i.e. a surface consisting of regular hexagons with carbon atoms at the vertices. The result of rolling depends on the orientation angle of the graphite plane in relation to the nanotube axis. This orientation angle determines the *chirality* of the nanotube, which governs, in particular, its electrical properties. This property of nanotubes is illustrated in Fig. 1a [35, 36], where a part of a graphite plane is shown and possible directions for its rolling are marked.

An ideal nanotube does not form seams in rolling and is ended with hemispherical caps containing not only regular hexagons but also 6 regular pentagons. Due to this latter peculiarity a nanotube can be considered as a limiting case of a fullerene molecule, whose length considerably exceeds its diameter.

The chirality of a nanotube is denoted by the pair of symbols (m, n) showing the coordinates of the hexagon on the graphite plane, which has to be superimposed on the origin hexagon as the result of rolling. Some of these hexagons are shown in the figure along with related labelling. Another way to specify the chirality consists in indication of the angle α between the direction of nanotube rolling and that of the common site of two adjacent hexagons. However in this case the diameter of the nanotube should be shown for the full description of its geometry.

The chirality indices of a single-walled nanotube (m, n) determine uniquely its diameter D. This relation is obvious and has the following form

$$D = \sqrt{m^2 + n^2 + mn}\ \frac{\sqrt{3}d_0}{\pi}\,, \tag{1}$$

where $d_0 = 0.142$ nm is the distance between neighboring carbon atoms in the graphite plane. The angle α is expressed through the chirality indices (m, n) by the relation

$$\sin\alpha = \frac{3m}{2\sqrt{n^2 + m^2 + mn}}\,. \tag{2}$$

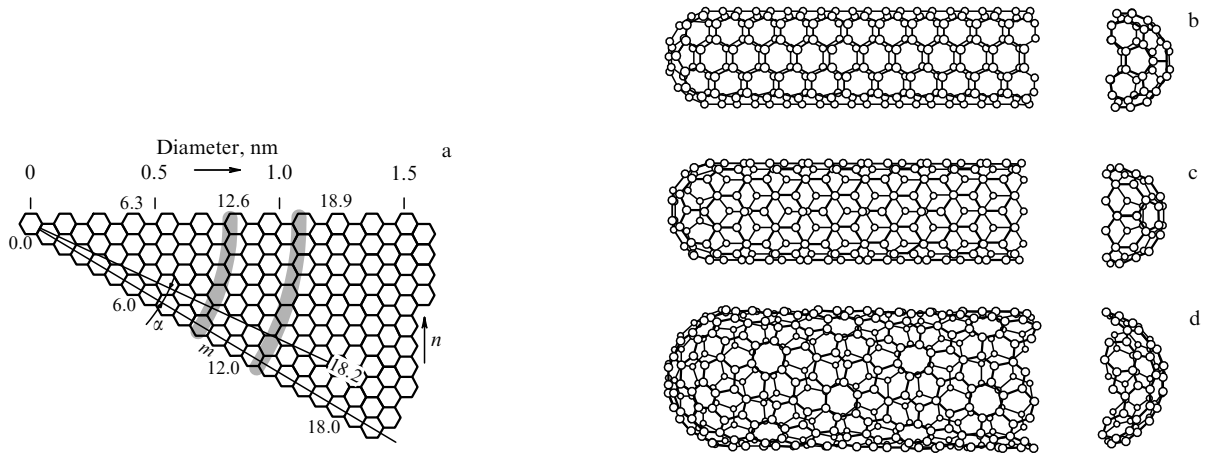

Figure 1. Illustration of the chirality of nanotubes [35, 36]: (a) a part of the graphite surface, the rolling of which into a cylinder results in the formation of a single-walled nanotube; (b) rolling at the angle $\alpha = 0$ gives the *armchair* structure; (c) rolling at the angle $\alpha = 30°$ corresponds to the *zigzag* structure; (d) a nanotube with chirality indices (10, 5).

Amongst different possible directions of nanotube rolling are distinguished those for which bringing of the hexagon (m, n) into coincidence with the origin requires no distortion in its structure. These directions correspond, particularly, to the angles $\alpha = 0$ (*armchair* configuration) and $\alpha = 30^\circ$ (*zigzag* configuration). Such configurations are specified by the chirality indices (m, 0) and ($2n$, n), respectively. The nanotube structures having *armchair* and *zigzag* configurations are depicted in Figs 1b and 1c. The nanotube structure with the chirality indices (10, 5) is shown in Fig. 1d.

Armchair nanotubes with chirality indices (10,10) take a special position among single-walled nanotubes. In such nanotubes, two of the C – C bonds incorporated into each of the hexagons are oriented parallel to the longitudinal axis of the tube. As follows from calculations [21, 22], nanotubes with such a structure should possess a purely metallic conductivity. Besides, the thermodynamic calculations [37] show that such tubes are distinguished by an enhanced stability and should prevail over nanotubes of other chirality in conditions where the single-walled nanotubes are predominantly formed. Until recently, such ideal conditions seemed to be unattainable. However, the theoretical conclusions have found an experimental verification in a first-rate work [37], where the metal-conductive single-walled nanotubes of 1.36 nm in diameter and up to several hundred μm in length were synthesized on irradiating a graphite surface with two laser pulses in the presence of a Ni/Co catalyst. As follows from electron microscope observations and X-ray diffraction measurements, nanotubes of predominant chirality (10,10) form bundles 5 – 20 μm in diameter, rolled into mats and tangled in an odd manner. Moreover, EPR-spectroscopy observations confirmed by direct measurements of conductivity in nanotubes point to the metallic character of electrical transport in these samples.

The experimentally examined structure of single-walled nanotubes differs in many respects from the above-presented ideal picture. First of all, this difference relates to nanotube caps whose structure is far from an ideal hemisphere, as follows from numerous observations.

Methods and results of experimental study of nanotube structure. Methods for experimental exploration of the structure of single-walled nanotubes have been developed. These methods based on conventional approaches to exploration of the structure of nano-sized objects include X-ray and neutron diffractometry, atomic field microscopy, scanning and high-resolution transmission electron microscopy, and also optical and Raman spectroscopy. The above-listed methods can be used mainly for the study of a large number of nanotubes with close structural parameters. The measurements can provide rather averaged structural characteristics of nanotubes but not a detailed analysis of properties of individual objects. Thus, in the first experiments of this kind [37, 38] bundles containing about a hundred single-walled nanotubes were used as the object of investigation. Observations performed through X-ray diffractometry and high-resolution transmission electron microscopy (TEM) have shown that the nanotubes involved in bundles are characterized by an ordered packing. This packing relates to the 2D triangular lattice with a parameter of 1.70 nm. Supposing the interlayer distance for adjacent nanotubes is close to 0.34 nm, as in crystalline graphite, the authors of papers [37, 38] were led to conclusion that such a lattice consists of similar nanotubes about 1.36 nm in diameter. It turned out to be quite alluring to assign to these nanotubes the chirality (10, 10) corresponding to their metallic behavior.

Nevertheless, further more detailed studies demonstrated that the structural parameters of single-walled nanotubes synthesized in real conditions are close, but not similar, to each other. Thus, Raman spectroscopy observations (see, for example, Ref. [39]) showed that the diameter of nanotubes involved in bundles can range between 1.1 and 1.5 nm. However, direct observations via high-resolution (HR) TEM [38, 40] have revealed that the distinction in structural parameters of nanotubes involved in a bundle is much less than that for nanotubes belonging to different bundles. Thus, the average diameter of nanotubes related to different bundles ranges between 1.44 and 1.74 nm. Such a distinction is caused by different synthesis conditions occurring in various plasma regions.

In this situation a necessity for developing methods of investigation providing the distribution of nanotubes over diameter and chirality parameters arises. One such a method is based on the use of electron diffraction from a spatial periodic structure, which is represented by a bundle consisting of several tens of single-walled nanotubes. Direct measurements of chirality of nanotubes synthesized by Thess et al. [37] were reported in one of the subsequent publications of the same group [41]. For this purpose the authors used an electron diffraction microscope with very small cross section of the electron beam (about 0.7 nm) quickly scanned over a region of 10 – 20 nm in diameter, filled with a bundle of nanotubes. The diffraction pattern obtained provides conclusions about the structure of the nanotubes comprising bundles. 35 bundles were studied with diameters ranging between 3 and 30 nm. All these bundles, except two, contained nanotubes of chirality close to (10,10). Detailed analysis showed that 44% of CNTs had chirality indices (10, 10), 30% — (11, 9), and 20% — (12, 8).

Further development of the electron diffraction method for detailed exploration of structural characteristics of single-walled nanotubes was undertaken in recent work [42], where this method was used in combination with HR TEM examinations. Single-walled nanotubes bound into bundles were produced on the surface of a cathode as a result of electric arc sputtering of graphite in a He atmosphere in the presence of a Ni/Y catalyst. Then the nanotube-containing soot was ultrasonicated in ethanol, whereupon it was situated on the grid of a transmission electron microscope. This allowed separation of isolated rectilinear bundles which were subjected to subsequent electron diffraction studies. As follows from the analysis of experimental data, single-walled nanotubes comprising an individual bundle are characterized by practically the same diameter, but distinctive (arbitrary) chirality. This statement is in contradiction with the conclusions of works [41, 43] but agrees with work [44].

The next step in investigation of structural features of single-walled nanotubes relates to employment of the scanning tunneling microscopy (STM) [45]. This has enabled a passage from the exploration of bundles containing nanotubes to the determination of the chirality of individual nanotubes. Nanotubes were produced using the conventional laser method based on laser irradiation of a graphite surface in the presence of a metal catalyst. The soot produced thereby contained single-walled nanotubes about 1.4 nm in diameter, bound in bundles. In order to untangle the bundles and separate individual nanotubes, the soot was dispersed in dichloroethane and then subjected to ultrasonic treatment.

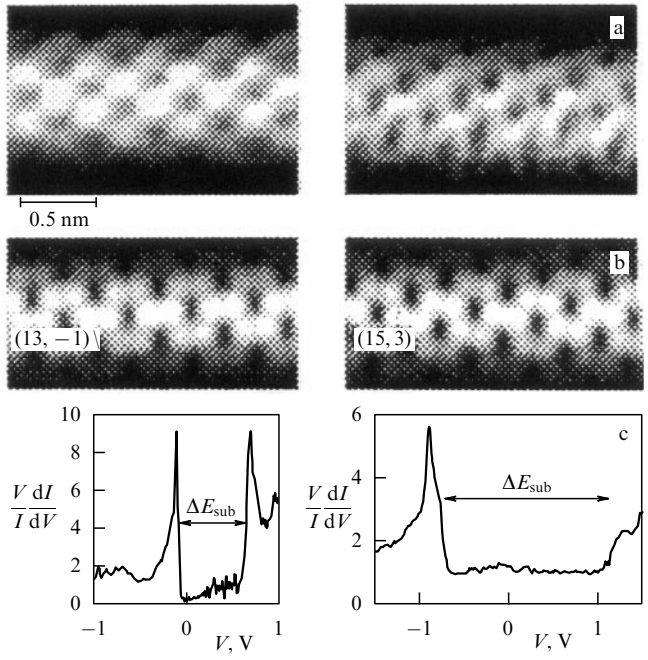

Figure 2. STM images and tunneling electron spectra of two individual single-walled nanotubes [45]: (a) images reconstructed on the basis of STM measurements; (b) images calculated for nanotubes with chirality indices (13, −1) and (15, 3); (c) maps of the density of occupied states, reconstructed on the basis of STM measurements and showing semiconductor properties of the nanotube 1, and metallic properties of the nanotube 2.

The nanotubes obtained in this fashion were placed onto an Au(111) surface which was used as a substrate in STM observations. These latter were performed at $T = 4$ K. Figure 2 displays representative STM images of two individual nanotubes distinguished from each other in diameter and chirality. One of these nanotubes is a semiconductor having an energy gap width of 0.80 eV, diameter of 1.0 ± 0.1 nm, chirality angle of $26 \pm 1°$, and chirality indices either (12, −1) or (13, −1). The second one possesses metallic conductivity and has a diameter of 1.27 ± 0.09 nm, chirality angle of $21.1 \pm 1°$, and chirality indices (15, 3). Thus, researchers have at their disposal the possibility of establishing all the parameters of a single-walled nanotube, which determine its electronic properties. The example cited illustrates a degree of uncertainty about structural parameters of individual nanotubes, which can be determined through the STM.

One more quite informative method for evaluation of structural parameters of single-walled nanotubes is based on Raman spectroscopy [46]. Figure 3 shows typical Raman spectra of a single-walled CNT, obtained using excitation laser sources of various wavelengths [47]. As is seen, the spectrum contains two groups of peaks, one of which (short-wave) is related to so-called tangential vibrations of carbon atoms in a graphite plane. These peaks with energy of 1590, 1566 and 1551 cm^{-1} are inherent only to single-walled CNTs and are practically unobservable in the case of multiwalled nanotubes. Thus, the existence of Raman peaks related to tangential vibrational modes implies unambiguously the presence of single-walled nanotubes in the sample.

Another group of lines distributed over the energy range of 150–250 cm^{-1} corresponds to so-called radial breathing modes. These are the vibrations of the nanotube diameter in relation to its mean value. The frequency of such vibrations is

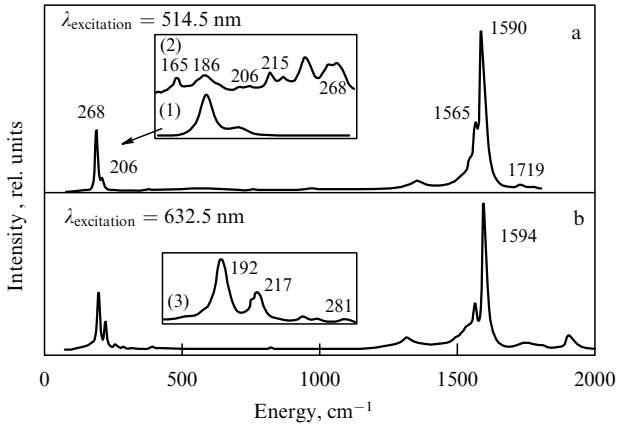

Figure 3. Raman spectra of samples containing single-walled nanotubes [47]: (a) wavelength of the exciting laser is equal to 514.5 nm; (b) 632.5 nm. An enlarged long-wavelength part of the spectrum, related to the radial breathing modes, is shown separately in the insets.

inversely proportional to the nanotube radius, and therefore this part of the Raman spectrum contains information about the nanotube diameter distribution. The interconnection between the diameter of a single-walled nanotube d (nm) and the position of the relevant Raman peak ω_d (cm^{-1}) is expressed by the following relation [46, 48]

$$\omega_d = \frac{223.75}{d}\,. \tag{3}$$

Application of this expression to the analysis of Raman spectra plotted in Fig. 3 leads to the conclusion that the sample under investigation contains, in particular, single-walled nanotubes with the diameters ranging between 1.06 and 1.2 nm. Besides, there are a small number of nanotubes with the diameters ranging between 0.83 and 1.36 nm.

As is stated in a recent work [49], information about structural parameters of single-walled nanotubes is contained not only in Raman spectra, but also in optical absorption spectra of samples. This considerably facilitates the procedure of evaluation of the nanotube diameter distribution, making it accessible to a much wider circle of researchers. Mutual relations between the diameter and the density of occupied electronic states cause an interconnection between the optical absorption spectrum of a single-walled nanotube and its diameter, as is illustrated, in particular, in Fig. 2.

Electron optical absorption spectra of samples containing single-walled nanotubes were obtained by Jost et al. [49]. These samples were synthesized as a result of laser sputtering of graphite in the presence of a Ni/Co catalyst. The synthesis was carried out in a chamber inserted into an oven whose temperature could be varied between 800 and 1260 °C. Before performing the spectral measurements, a soot containing nanotubes was admixed to methanol in the weight ratio 1:100 and ultrasonicated [50]. Then the solution was spread through a sprayer onto a quartz plate, the temperature of which was kept at 70 °C. The absorption spectrum of the film obtained after extracting the background is depicted in Fig. 4. Peaks A and B are related to transitions between singularities on the map of density of occupied states of semiconducting nanotubes, whereas peak C corresponds to that for metallic nanotubes. A notable temperature dependence of the spectrum is observed, so that a lowering in the oven temperature results in a shift of the positions of all the peaks towards the

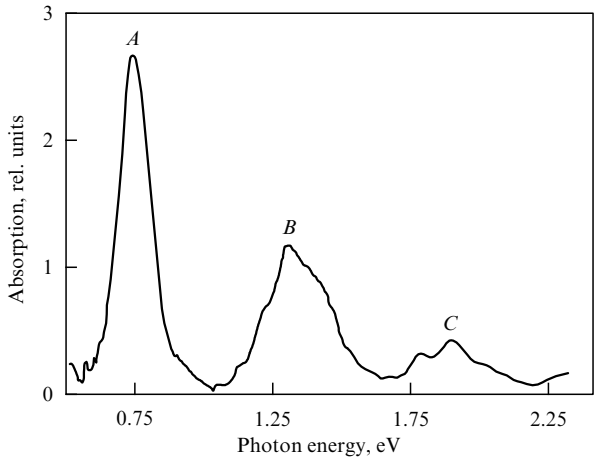

Figure 4. Typical optical absorption spectra of a material containing single-walled nanotubes [49].

high-energy region. Enhancing the ratio Ni/Co causes a similar shift. Processing the optical spectra provides not only the mean diameter of nanotubes, but also parameters of their diameter distribution. Thus, the width of the spectral peak *A* determines the width of this distribution. The nanotube content in the sample and nanotube diameter distribution function versus oven temperature and catalyst content, evaluated as a result of treating the spectral peak *B*, are presented in Fig. 5. As is seen, the diameter distribution ranges between 1.01 and 1.42 nm. This distribution is shifted in the direction of increasing diameter as the synthesis temperature rises and the content of Ni in the catalyst decreases. This points to the possibility of controlling the diameter of single-walled CNTs produced through variations in the synthesis temperature and the catalyst content.

The fine structure of the optical absorption spectra contains equidistantly situated peaks corresponding to a change $\Delta d \approx 0.07$ nm in the diameter of a nanotube, as follows from the expression

$$d = \sqrt{m^2 + n^2 + mn}\,\frac{\sqrt{3}d_0}{\pi}$$

used at $m \sim n$ (the chirality angle is about 30°). Therefore one can conclude that nanotubes of armchair structure prevail in the sample, which is in an agreement with the character of Raman spectra.

Single-walled nanotubes of the smallest diameter. Analyzing structural peculiarities of single-walled nanotubes an interesting question arises. It concerns the smallest possible diameter of a nanotube and also the possibility of synthesis and stable existence of nanotubes with such a diameter. This question was first formulated shortly after the discovery of nanotubes in work [51], the authors of which related the diameter of the nanotube with that of the relevant fullerene molecule closing this nanotube. In particular, the diameter of the most abundant nanotube of *armchair* structure and chirality indices (10, 10) is about 1.36 nm, which is close to that of the fullerene molecule C_{240} having an enhanced stability as well. However, nanotubes of 0.7, 0.47 and 0.39 nm in diameter, which should be closed with quite symmetrical and stable fullerene molecules C_{60}, C_{36} and C_{20}, were not observed until recently. The structure of these nanotubes is depicted in Fig. 6.

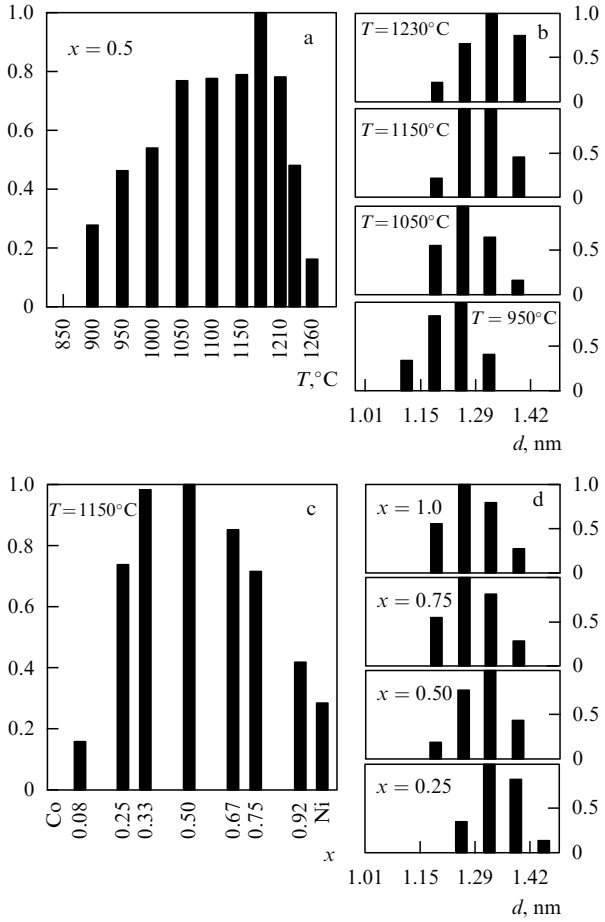

Figure 5. Results of processing the optical absorption spectra of samples containing single-walled nanotubes produced at various oven temperatures and Ni_xCo_{1-x} catalyst content [49]: dependences of the relative nanotube yield on the oven temperature (a) and catalyst content (c); nanotube diameter distributions at various oven temperatures (b) and catalyst content (d).

The question about the smallest possible nanotube diameter was somewhat clarified in the series of recent publications [52 – 56] reporting on the synthesis of nanotubes with the above-mentioned parameters. These studies were probably stimulated by the recent work [57], where the smallest possible fullerene molecule C_{20} was first synthesized through a sequence of gas-phase reactions.

The result of work [52], where a single-walled nanotube of 0.33 nm in diameter was synthesized and examined, seems to be the most impressive in this field. This nanotube with probable chirality indices (4,0) is incorporated into the heterojunction (11, 11) – (4, 0) – (11, 11) which is the smallest p – n junction produced up to now. The nanotubes were extracted from cloth-like soot produced through the electric arc method. The material was purified using the conventional methods and studied by means of an HR TEM and Raman spectrometer. The measurement data show that the sample contains nanotubes with diameters ranging between 0.5 and 1.55 nm. Irradiation of the point of crossing of two (11, 11) nanotubes with the electron beam of a TEM for 10 s results in the appearance of a joining nanotube of 0.33 nm in diameter with chirality indices (4, 0).

Single-walled nanotubes with the smallest attainable diameter (0.4 nm) were synthesized in work [56] through the pyrolysis of tripropilamine in pores of the monocrystalline

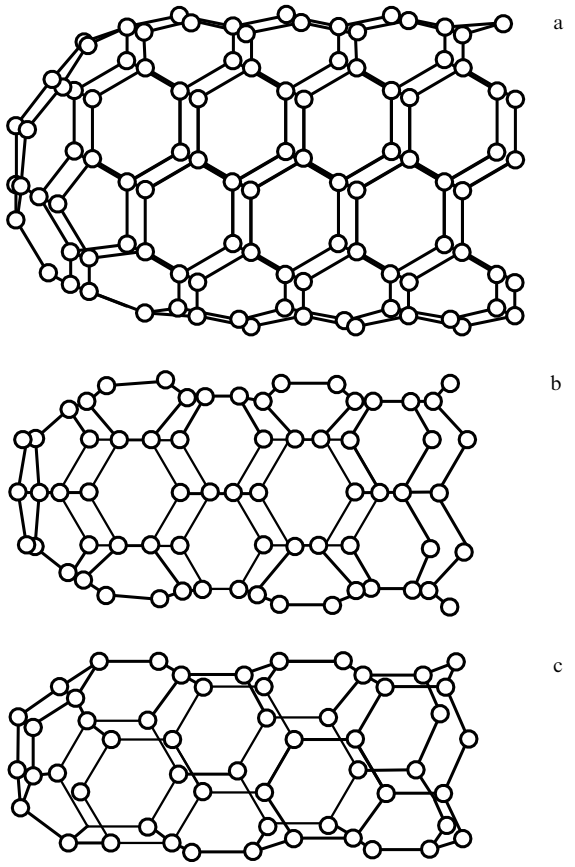

Figure 6. Structure of single-walled nanotubes of 0.7 (a), 0.47 (b) and 0.39 nm (c) in diameter, closed with fullerene molecules C_{60}, C_{36} and C_{20}, correspondingly [55].

ions with an energy of tens of electron-volts onto a substrate surface at a temperature of 150 °C [55]. These nanotubes consisted of 10–15 layers separated by 3.4 nm. HR TEM observations make it possible to distinguish a single-walled nanotube of 0.39–0.40 nm in diameter inside many nanotubes.

2.2 Multiwalled nanotubes

Multiwalled nanotubes are distinguished from single-walled ones by their considerably wider diversity of shapes and configurations. The structural diversity reveals itself in both longitudinal and transverse directions. Possible modifications of the transverse structure of multiwalled nanotubes are presented in Fig. 7 [58]. The 'Russian doll' structure (Fig. 7a) is an assembly of single-walled cylindrical tubes coaxially stacked one into another. The other version of this structure, shown in Fig. 7b, is a set of coaxial prisms stacked one into another. Finally, the last of the structures presented (Fig. 7c) looks like a scroll. For all the structures shown the magnitude of inter-layer spacing is close to 0.34 nm, which is inherent to that in crystal graphite.

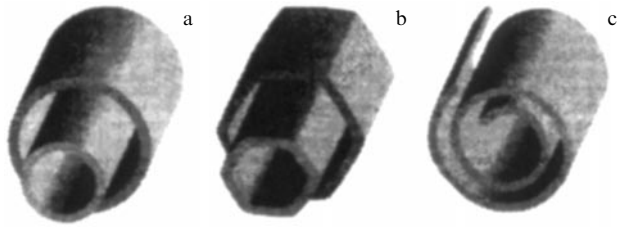

Figure 7. Models pertaining to transverse structures of multiwalled nanotubes [58]: (a) 'Russian dolls'; (b) hexahedral prisms; (c) the scroll.

zeolite $AlPO_4$-5. This transparent microporous material contains 1D channels of 0.73 ± 0.01 nm in diameter, forming a hexagonal matrix. Tripropilamin was inserted into the channels during the crystal growth. The nanotubes are formed inside zeolite channels as a result of thermal treatment of carbon which is a product of the pyrolysis. The nanotubes produced were dissolved in 30% HCl and observed by means of an HR TEM. Ultrathin nanotubes of 0.42 ± 0.02 nm in diameter can be discriminated in the image. These nanotubes were destroyed for 10–15 s under the action of the electron beam of TEM. One can imagine 3 types of single-walled CNTs with diameters close to 0.4 nm: *zigzag* (5, 0) (diameter 0.393 nm); *armchair* (3, 3) (diameter 0.407 nm), and a nanotube of chirality (4, 2) (diameter 0.414 nm). *Zigzag* (5, 0) closed with half of the fullerene molecule C_{20} seems to be the most probable structure.

Electric arc synthesis of nanotubes was performed in work [54] in an H_2 atmosphere without any metal catalyst. An HR TEM image of the sample contains an 18-layer nanotube with an inner tube of 0.4 nm in diameter in its interior. Certain of such inner tubes have an *armchair* structure (3, 3). They are ended with a fullerene hemisphere making up half of the dodecahedron C_{20}, where the angle between the two C–C bonds measures 108°, which is close to the relevant angle in the sp^3 configuration of diamond.

Single-walled nanotubes situated inside multiwalled cylindrical structures were observed in some works along with isolated nanotubes of minimum size. These multiwalled nanotubes were obtained as a result of deposition of carbon

The realization of one or other type of structure in a specific experiment depends on the nanotube synthesis conditions. The analysis of available experimental data indicates that the most characteristic structure of multiwalled nanotubes is the 'Russian doll' structure (Fig. 7a), in which tubes of a lesser diameter are inserted successively into those of a larger diameter. Compelling direct evidence of such a structure has been demonstrated in the recent publication [59], the authors of which managed using a special manipulator to extract the inner layers of a nanotube, keeping the outer ones fixed. In doing so the nanotube can be extended and shortened, like a telescopic antenna or fishing-rod. The scheme of the experiment mentioned is illustrated in Fig. 8. One end of a multiwalled nanotube of 35 nm in diameter was attached to a grounded gold electrode. The second one was connected to another nanotube which was subjected to a varied voltage and played a role of the forming electrode. Supplying a voltage of several volts on this electrode being in contact with the nanotube resulted in a current of several hundred mA, followed by a removal of several layers from the nanotube near its cap and sharpening of the nanotube end. This resulted in a decrease in the number of nanotube layers near an end part down to three, and its diameter down to 2.5 nm. Such a sharpened nanotube is, in particular, almost an ideal tip for an atomic field microscope.

Figure 8 shows the manner in which the manipulation with a nanotube is performed. A nanotube with one fixed end (Fig. 8a) is subjected to the procedure of sharpening using an electric current (Fig. 8b). In all the following

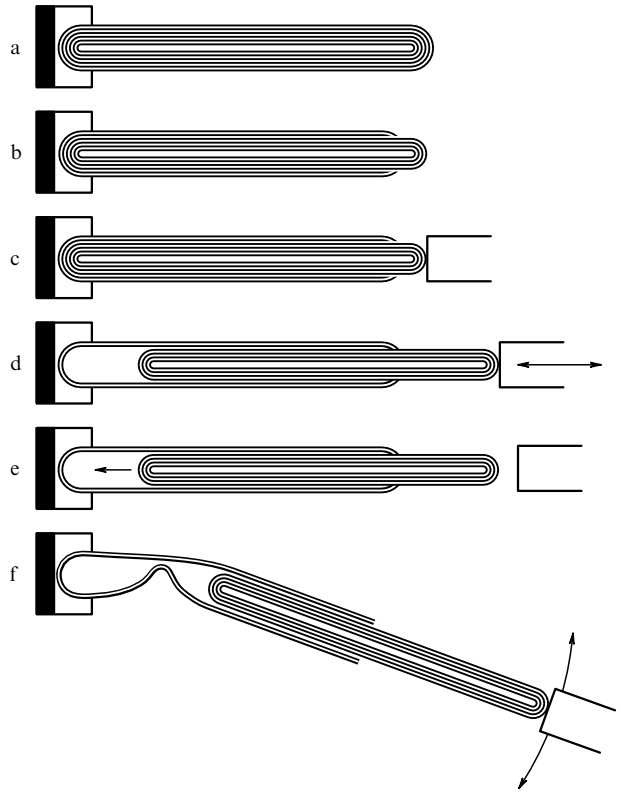

Figure 8. Schematic representation of the experiment on lengthening and sharpening multiwalled nanotubes [59]: (a) original nanotube; (b) the nanotube after the procedure of electrothermal removal of outer layers from the tip; (c) the nanotube with the spot-welded manipulator; (d) the manipulator's movements cause reversible displacements of inner layers of the nanotube relative to outer ones; (e) removing the manipulator results in a spring-like return of inner layers of the nanotube into the original position; (f) transverse displacements of the manipulator promote a reversible bending of hollow outer layers of the nanotube.

manipulations the sharpened nanotube end is contacted to a manipulator (Fig. 8c). Moving the manipulator in the longitudinal direction results in a reversible expansion or shortening of the nanotube due to extraction of its inner core out of the outer shell (Fig. 8d). This procedure can be performed repeatedly under the control of TEM. A quick removal of the manipulator from the extracted inner core results in a spontaneous retraction of the core due to the action of van der Waals attractive forces between nanotube layers (Fig. 8e). A transverse force acting on partially extracted inner core causes its bending, which becomes irreversible at some excess of critical load (Fig. 8f). Using the measured retraction time of the extracted inner core, the magnitudes of static (2.3×10^{-14} N atom^{-1}) and dynamic (1.5×10^{-14} N atom^{-1}) friction force acting between layers were estimated. It was observed that the action of a transverse force on a multiwalled CNT results in easier bending, if the inner core is partially extracted out of the outer shell. Thus, one particular nanotube of 43 nm in diameter, consisting of 60 graphite layers, was telescoped so that an inner fragment of 29 nm in diameter, consisting of 40 layers, was pulled out up to a maximum extension of 150 nm. The transverse bending of such a telescopic tube by 5° resulted in the formation of a kink in the middle of the section with a larger inner diameter (Fig. 8f). A force causing a bend of 26° was followed by destruction of the tube. At bending angles less than 10°, the extracted part of the nanotube can be retracted back, accompanied by smoothing the deformation. A higher bend hindered the retraction of the extracted part of the nanotube into the initial position.

Another experiment directed to establishing the structure of a multiwalled nanotube is described in works [60, 61]. In these works, the possibility was first demonstrated for the intercalation of K atoms and $FeCl_3$ molecules inside carbon nanotube bundles to modify the electronic structure of nanotubes. It was found that this possibility is largely dependent on the conditions of the nanotube production.

Multiwalled nanotubes produced in two ways were used as a starting material: in a graphite-electrode arc discharge and through the chemical vapor deposition with iron and nickel particles as a catalyst, as described by Yudasaka et al. [62]. In the first case, spatially aligned multiwalled nanotubes several tens of nm in outer diameter were produced, being closely packed in bundles which in turn formed thread-like structures up to 3 mm in length and 0.1 mm in diameter. In the second case, the subject of study was a bundle of disordered multiwalled nanotubes several tens of nm in outer diameter applied upon a glass substrate. Intercalation was performed in a two-section glass tube. Nanotubes were suited in one section, whereas an intercalated agent was put into another one. Either purified K or anhydrous iron chloride ($FeCl_3$) was used as an intercalated agent. The tube was pumped out and sealed off. The gas-phase reaction was proceeded at a temperature of 300 °C in the case of K, and 280 °C in the case of $FeCl_3$. All the procedures were carried out in a sealed off chamber in an Ar atmosphere.

It should be noted as the main result of the cited publications [60, 61] that the intercalation could be performed only in relation to samples produced using the electric arc method. The intercalation reaction did not change either the dark color or thread-like structure of samples, while in the case of $FeCl_3$ some deterioration and desorientation of fibers was observed. The samples were notably increased in weight (15 – 33% in the case of K, and 110 – 260% in the case of $FeCl_3$) and size. The intercalation reaction considerably changed the appearance of nanotubes viewed under a scanning electron microscope. Straight nanotubes become convex as a result of the reaction, especially in the case of $FeCl_3$. The results of X-ray diffraction investigations showed that the intercalation causes an increase in the interlayer spacing from 0.344 up to 0.53 nm in the case of K, and up to 0.95 nm in the case of $FeCl_3$. This proves that the intercalation affects each nanotube, but not the intertube region. The intercalated nanotubes are shaped into beadline or bamboo-like patterns, where the swollen sections alternate nonintercalated 'necks'. This proves that the nanotubes produced through the electric arc method have a scroll structure and are intercalated from the lateral seam but not from the end side. The nanotubes produced through the chemical vapor deposition method are not affected by the intercalation reaction in the conditions described above. Therefore, the authors of the experiment concluded that in this case the structure of nanotubes is close to the 'Russian doll' one.

One should bear in mind that the perfect transverse structure of nanotubes, where the interlayer spacing is close to 0.34 nm and axially independent, is distorted in practice due to the perturbing action of adjacent nanotubes. This was demonstrated in one of the first publications on the subject [63], where the electron microscope observations showed a

2–3% decrease in interlayer spacing in the area of contact between 10-layer and 12-layer adjacent nanotubes. The estimates taking into account van der Waals interaction between carbon atoms confirm this effect quantitatively.

Other deviations from the ideal structure of multiwalled nanotubes were observed in works [64–68] using the electron microscopy and X-ray diffraction methods. Thus, high-resolution electron microscope observations [65, 66] have shown that a considerable portion of multiwalled nanotubes have a polygonized cross section. In such a structure, the plane sections are adjacent to surfaces of high curvature, which contain edges with a high degree of sp^3-hybridization of carbon. These edges confine the surfaces consisting of sp^2-hybridized carbon and determine many properties of nanotubes. The impact of sp^3 defects on the ideal structure of the nanotube surface was studied in more details in works [67, 68]. It was shown, in particular, that the defects cause a distortion in the rectilinear form of the nanotube, shaping it in a pleat-like structure whose wavelength is 2–8 times as large as the six-member ring size.

A great deal of information about the transverse structure of multiwalled nanotubes was provided by work [69], where in contrast to the conventional approach the electron beam in diffraction measurements was aligned in parallel to the nanotube axis. Let us consider this work in more details. Nanotube bundles extracted from a cathode soot were inserted into an epoxide resin with tweezers. After solidification at 60 °C for 3 days the plane samples 20–30 nm in thickness were cut from the resin bulk with a diamond knife and examined using a high-resolution electron microscope. The observations showed that one end of a tube is usually connected with a piece of the pyrolytic graphite or the polyhedral particle. The other end of the nanotube is closed, while its shape is closer to a cone rather than to a sphere. A wide diversity of tube configurations was established. Thus, a seven-layer tube 2.04 nm (6×0.34 nm) in inner diameter was seen. The interlayer spacing was always close to 0.34 nm. A 32-layer tube having an inner diameter of 3.4 nm (10×0.34 nm) might also have been seen. A rise in the number of layers results in an increased deviation from the ideal cylindrical shape of a nanotube. In some cases a polyhedral structure of the outer envelope of a nanotube was observed. Sometimes a nanotube surface was covered with a thin layer of disordered (amorphous) substance. The ideal closed concentric structure of the cross section was viewed in none of the cases.

Both the longitudinal and transverse structures of multiwalled nanotubes significantly depend on the production method. As was found in works [58, 70–73] using electron diffraction methods, the widest diversity of longitudinal structures is inherent to multiwalled nanotubes grown on the surface of metal nanoparticles through catalytic acetylene decomposition. Catalytically grown nanotubes usually have an inner and outer diameter of several nm and several tens of nm, correspondingly, and reach up to several tens of microns in length. About 10% of nanotubes are formed into regular spirals with the radius and pitch varied over wide limits. The tubes curve in an odd manner; they are twisted with themselves and with each other, forming twisted spirals, ropes, loops and structures of all other sorts.

Observations have shown that the interlayer spacing in a multiwalled CNT produced in an arc discharge can change from the standard value of 0.34 nm to twice the magnitude, 0.68 nm. This implies the existence of defects in nanotube structures, where one or more of the layers is partly or fully absent.

Another sort of defects observed quite often on the graphite surface of multiwalled nanotubes is a result of inclusion of a number of pentagons or heptagons into such a surface consisting mainly of regular hexagons. The presence of these defects in the structure of nanotubes causes distortion in their cylindrical shape, so that the inclusion of a pentagon brings a convex bend, whereas a heptagon produces a concave bend of the ideal cylindrical surface of the nanotube. Therefore, such defects result in the appearance of curved and spiral-like nanotubes. The existence of spirals with a constant pitch is indicative of a more or less regular arrangement of defects on a nanotube surface. This problem was studied in detail, in particular, in work [74], where on the basis of observations of bent nanotubes a conclusion was made about the existence of seven-member carbon rings in their structure. The nanotubes were produced in conditions typical of fullerene production. A cathode deposit consisted of a black core surrounded with a gray cylindrical envelope. The core was inserted into methanol and ultrasonicated for 10 min, resulting in a black suspension. On drying the latter a black powder was obtained, containing nanotubes, polyhedrals and amorphous carbon. The gray envelope of the deposit essentially did not contain nanotubes. Bent nanotubes were observed directly using a high-resolution electron microscope 300 kV in voltage and 0.20 nm in resolution, designed on the basis of a field emission microscope. The minimum diameter of the electron beam was 3 nm. Bent nanotubes were observed, which implied the occurrence of sections of negative curvature caused by the presence of heptagons or pentagon–heptagon pairs in the graphite structure. A nanotube bend is accompanied by either bending or breaking of a graphite surface.

3. Methods for the production of CNTs

CNTs are formed as a result of high-temperature chemical transformations of carbon-containing materials. There is a wide variety of conditions promoting these transformations. Correspondingly, the set of methods used for nanotube production is also quite large. A detailed description of these methods can be found, for example, in the earlier review of the author [8], and also in the subsequent review article [40]. This article contains only a description of the most widely used methods for the solution of this problem, providing large-scale synthesis of CNTs. These methods have been subjected to a continuous modification recently, which will be considered in detail below.

Electric arc sputtering of graphite. The most widespread method for synthesis of CNTs is based on the utilization of the electric arc discharge with graphite electrodes, burning in an inert gas atmosphere (usually helium). This method was developed by Kratschmer and collaborators for large-scale fullerene production [2] and was, in particular, used in the pioneering work of Iijima [7], where carbon nanotubes were first observed in products of thermal decomposition of graphite in an electric arc.

A typical electric arc facility for the production of a material containing fullerenes and nanotubes is shown schematically in Fig. 9a [40]. The arc discharge between graphite electrodes is burning in a chamber with water-cooled walls at a buffer gas (He or Ar) pressure of about 500 Torr. The interelectrode gap is held constant at the level

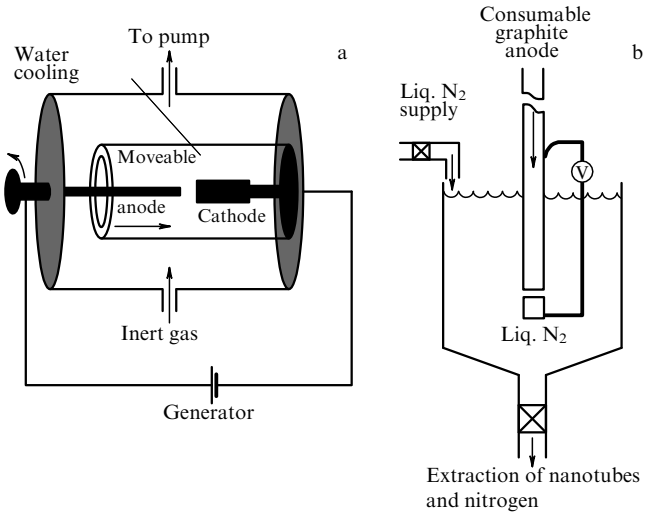

Figure 9. Schematic representation of the electric arc setups for synthesis of carbon nanotubes in gram quantities: (a) Kratschmer scheme [40]; (b) a modified Kratschmer scheme with the use of liquid nitrogen [75].

of about 1 mm. The plasma temperature in an interelectrode region reaches about 4000 K at an arc current of about 100 A and an applied voltage range between 25 and 35 V. The temperature of the graphite anode surface, subjected to an intense vaporization, is characterized by the same magnitude. Convection caused by a considerable temperature difference across the near electrode plasma region results in the removal of carbon atoms from a hot to a colder plasma region, where their sublimation occurs. A part of the carbon material formed as a result of sublimation is shaped into elongated cylindrical structures consisting of a graphite plane rolled into a tube. This material is deposited on either the water-cooled surface of a discharge chamber or the cathode surface facing the anode.

An interesting modification of the electric arc method intended for the production of CNTs was realized in recent publication [75]. The layout of this setup is depicted in Fig. 9b. Electrodes are arranged vertically and immersed into liquid nitrogen, where a district current arc discharge is burnt. Both the interelectrode gap and the level of liquid nitrogen were fixed automatically. A long graphite rod 0.6 cm in diameter was used as an anode, and a graphite rod 1.2 cm in diameter was utilized as a cathode. The nanotube synthesis was carried out at an arc current of 60 A, and voltage of 20 – 25 V. Arc burning results in a transformation of the anode material into a deposit covering the bottom of the chamber and consisting mainly of multiwalled (4 – 8 layers) nanotubes. The total yield of the material containing nanotubes reached 44 mg min^{-1} (per 1 cm^2 of the anode surface) at a consumption of liquid nitrogen of 0.2 l min^{-1}. As follows from the analysis performed using the tunnelling electron microscopy and electron energy loss spectroscopy, the material obtained is characterized by a quite high content of nanotubes and does not require practically any subsequent purification. The advantages of the described method of nanotube production relate to the simplicity of its realization and the possibility of scaling the facility for increased production.

The properties of nanotubes formed as a result of the electric arc sputtering of graphite depend largely on the presence or absence of catalyst particles in the region of synthesis. Catalysts were not used in the first several years of development of nanotube research. The soot formed on a cathode surface as a result of arc discharge burning contains multiwalled nanotubes along with fullerenes and nano-sized polyhedral graphite particles. This soot appears like either flakes or a powder. TEM observations show that the nanotubes reach about 1 μm in length and contain from a few up to several tens of concentric graphite layers spaced from each other at 0.34 nm, which is the interlayer distance in crystalline graphite. The inner diameter of nanotubes ranges between 1 and 3 nm, depending on the number of layers, whereas the outer diameter ranges between 2 and 25 nm.

The presence of catalyst particles considerably affects the structural and other characteristics of the nanotubes synthesized. The most widely used method of inserting metal catalyst particles into the electric discharge plasma consists in filling a longitudinal hole drilled in an anode rod with a mixture of a metal powder and finely dispersed amorphous carbon. This mixture is impressed into the hole facing the cathode. Both individual elements (Co, Ni, Fe, Cu, Mn, Li, B, Si, Cr, Zn, Pd, Ag, W, Pt, Y and Lu) and double and even triple mixtures of these elements are used as a catalyst. Thus, in the above-cited work [47] samples of a material containing single-walled nanotubes were produced in an electric arc at a 0.66-atm pressure of He. A graphite rod 6 mm in diameter, containing a longitudinal cylindrical hole, was employed as an anode. This hole was filled with a mixture of CeO_2, powdered Ni (grain size < 100 nm) and graphite with a molar ratio 1:4:95. Before the experiment, the anode rods were conditioned for 2 hours in an Ar atmosphere at 200 °C. The discharge was burnt at a current of 100 A and voltage 50 V. The deposit containing single-walled nanotubes shaped a collar-like mat. This mat was purified for 0.5 – 2 hours by means of concentrated nitric acid, washed with distilled water and dried in an Ar flow. Then the sample was annealed at 1000 °C for removal of volatile oxides covering its surface. The acid treatment resulted in a notable decrease in the size of the sample. Raman spectroscopy observations performed before and after the purification procedure showed some increase in the content of nanotubes in the soot as a result of purification, but do not indicate any notable changes in the Raman spectra. Spectra of radially breathing modes imply the presence of single-walled CNTs of 0.79 nm in minimum diameter. The cathode deposit formed with the use of a catalyst contains single-walled graphite nanoparticles, and also metal particles encapsulated inside one or several graphite shells, along with single-walled and multiwalled nanotubes. The highest abundance of single-walled nanotubes is inherent to the outer cylindrical region of the cathode deposit.

Long-term arc discharge burning results in the formation of material containing nanotubes not only on the front surface of the cathode, but also on water-cooled sections of gas-discharge chamber walls. This material forms a dense flexible structure resembling a sheet of a paper or a rubber in its appearance. It possesses quite high mechanical characteristics and can easily be separated from the chamber walls. Sometimes this structure is called *bucky-paper*. The content of nanotubes in such a structure can reach 20 – 25%.

At the moment, the efforts of researchers involved in the technology of nanotube production are focused on the enhancement of the process productivity and lowering the cost of the final product, correspondingly. The solution of this problem will offer opportunities for large-scale use of

CNTs in various fields of electronics, materials production, etc. In this connection one should note the recent work [76], where some modifications of the electric arc method for the production of nanotubes resulted in an extraordinary high productivity of the process.

In the above-cited work CNTs were synthesized in an electric arc chamber at a current ranging between 50 and 100 A, and a He pressure of 400–700 Torr. An elongated graphite rod 6 mm in diameter was utilized as a cathode. A similar rod, used as an anode, contained admixtures of Ni (4%) and Y (1%). A distinguishing feature of the facility is the arrangement of the electrodes which comprise an angle of about 30° as contrasted to the conventional parallel orientation. This provides the formation of a plasma jet several centimeters in size in the vicinity of the electrodes, which promotes removal of soot from the cathode surface and increases the yield of single-walled nanotubes in the products of plasma sputtering of graphite. Discharge burning results in the formation of a cloth-like layer of deposit on the walls of the chamber. Besides, a small amount of a finely dispersed deposit is built up on the lateral surface of the cathode, and a hard formation resembling the tail of a comet is observed on the edge surface of the cathode.

The measured rate of vaporization of the anode material at a current of 100 A reaches 1.24 g min^{-1}. The cloth-like deposit therewith comprises about 80% of the total mass lost by the anode. As follows from TEM and scanning electron microscopy observations, and also from the Raman spectra of the samples obtained, the deposit formed on the lateral surface of the cathode practically does not contain single-walled nanotubes. The relative content of single-walled nanotubes in the hard formation on the edge surface of the cathode is quite high. However, the mass of this formation does not exceed 6% of the total loss in mass of the anode, so that the contribution of that region to nanotube production is relatively low. The cloth-like deposit formed on the discharge chamber walls contains up to 50 wt.% of single-walled nanotubes (ranging between 1.28 and 1.58 nm in diameter) bound into bundles, as well as particles of metal, amorphous carbon and graphite, and single scales of a graphite layer. Therefore, the presented modification of the electric arc method for the production of single-walled nanotubes provides an enhancement of productivity of the process by as much as several times in comparison with the conventional approach without lowering the nanotube yield.

Ablation of graphite using laser or solar irradiation. Laser irradiation of a graphite surface in a buffer gas atmosphere [12] is used for nanotube production along with the electric arc thermal sputtering of graphite. Just this method was used in the pioneering work [1] which resulted in the discovery of fullerenes and subsequently won the Nobel Prize for Chemistry [4–6]. The experimental setup is shown schematically in Fig. 10a [40]. A graphite target 2.5 cm in diameter is placed into a long quartz tube 5 cm in diameter and 60 cm in length, which in turn is inserted inside a cylindrical oven 30 cm in length and heated up to a temperature of about 1000 °C. As a buffer gas, helium or argon at a pressure of about 500 Torr was utilized, flowing along the tube rather slowly. Irradiation of the edge surface of the target was carried out by means of a Nd:YAG laser with a pulse duration of 8 ns. The diameter of the focus spot was 1.6 mm. The total irradiation energy, including both the first ($\lambda = 1.06$ μm) and second ($\lambda = 0.532$ μm) harmonics, comprised 140 mJ. The evolution dynamics of the torch arising as a result of laser ablation was studied by means of nonfocused time-delayed XeCl laser pulses ($\lambda = 308$ nm) 30 ns in duration and 20 mJ cm^{-2} in power density. The emission of the torch was spectrometered and photographed at various phases of its evolution. Products of the thermal sputtering of graphite were carried away with a buffer gas from a hot region and were deposited onto the water-cooled surface of a copper collector. These products contained fullerenes, nano-sized graphite particles and also multiwalled nanotubes up to 300 nm in length with the number of layers ranging between 4 and 24.

Inserting a metal catalyst inside a graphite rod provides predominant formation of single-walled nanotubes as a result of laser ablation of the graphite [37]. In this relation the best version of catalyst is a double alloy containing Ni, Co, Fe, Y and Pt. The optimum content of the catalyst material in the graphite target is 1–2 at.%. The maximum yield of single-

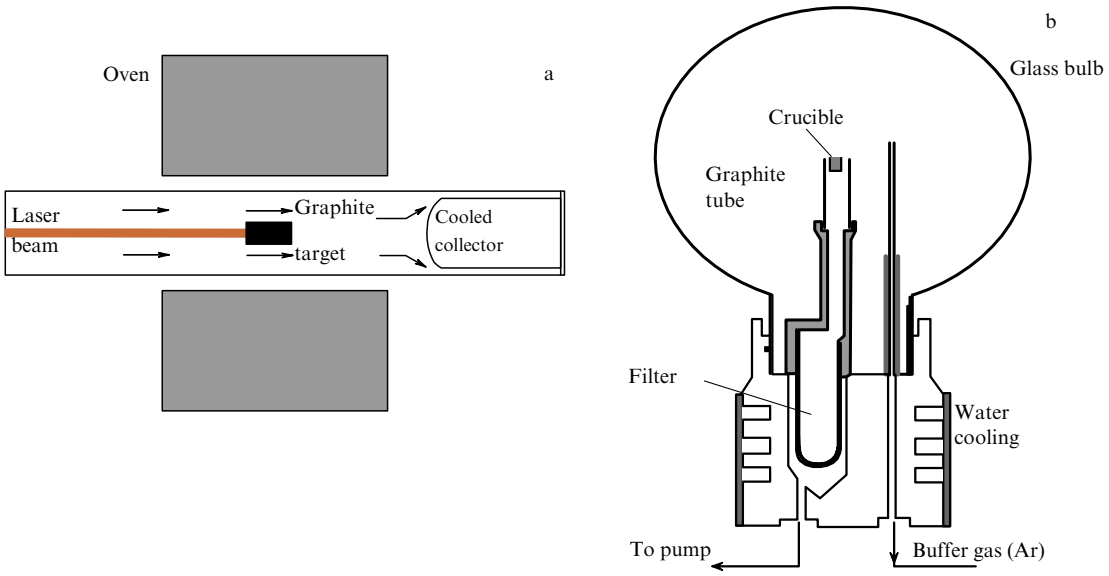

Figure 10. Schematic representation of methods for the production of fullerenes and nanotubes, based on the ablation of a graphite target under the action of light irradiation: (a) laser ablation [8]; (b) ablation as a result of solar irradiation [40, 79].

walled nanotubes in the deposit reaches 90%. The deposit also contains nanoparticles and amorphous carbon particles along with nanotubes.

The most interesting results are provided by the application of a sequence of two laser pulses ensuring more homogeneous heating of the target material. In certain conditions (pressure and sort of a buffer gas, laser irradiation intensity), the diameter distribution of nanotubes produced is rather narrow and has a maximum near 1.4 nm. This corresponds to the chirality indices (10, 10). The nanotubes are arranged in a regular manner into bundles of about 10 nm in diameter, which contain about hundred individual tubes.

An important distinctive feature of the laser method for CNT production relates to the high sensitivity of the properties of nanotubes synthesized to the parameters of the laser irradiation. In particular, this feature was clearly demonstrated in work [77], where an interconnection between the peak intensity of laser irradiation of the target surface and mean diameter of nanotubes formed was established. A pressed mixture of a graphite powder 4 μm in grain size and finely dispersed powder of Co and Ni each of 0.6 at.% in content was used as a target. The target subjected to a preliminary thermal treatment was inserted into a quartz tube which in turn was situated in an oven heated up to 1200 °C. The target surface was irradiated with pulses of a Q-switched Nd:YAG laser ($\lambda = 1.06$ μm). The laser beam was focused onto a spot 0.86 mm^2 in area, which provided an average intensity of the target cw-mode irradiation of up to 3.5 kW cm^{-2} and a peak intensity in a pulsed mode ranging between 0.2 and 3.5 MW cm^{-2}. The intensity of the target irradiation was controlled by variation of the pulse duration and repeating frequency. Argon at a pressure of 500 Torr was utilized as a buffer gas. The products of laser sputtering of the target were studied using TEM and Raman spectrometry.

The results of these studies showed a strong dependence of the diameter distribution of CNTs on both the pulse duration and peak intensity of laser irradiation. Thus, at a pulse duration of 575 ns, corresponding to the peak irradiation intensity of 0.2 MW cm^{-2}, the Raman spectrum displayed a predominance of nanotubes 1.22 and 1.08 nm in diameter with chirality indices (9, 9) and (8, 8), respectively. Increasing the peak irradiation intensity up to 0.9 MW cm^{-2} resulted in a rise of the yield of nanotubes with chirality indices (8, 8) and also in the appearance of a small quantity of those 1.35 nm in diameter with chirality indices (10, 10). The content of the latter is as low as twice that for (8, 8) and (9, 9) nanotubes. In this case the average diameter of nanotubes was slightly decreased. This trend of decreasing the average diameter of nanotubes with rising laser irradiation intensity is retained on increasing the irradiation intensity up to 1.5 MW cm^{-2}. In this case nanotubes 1.08 nm in diameter, having the chirality indices (8, 8), prevail.

The above-cited work demonstrated the possibility of an aimed synthesis of CNTs with pregiven structural parameters. This possibility comprises one of the main advantages of the laser method for nanotube synthesis. The disadvantages refer to its relatively low productivity and difficulties arising in scaling.

Subsequent studies [78] have shown that not only rare gases (He, Ar) can be used as a buffer gas, but also the considerably more widely available N_2. The experiments were curried out at a graphite surface temperature of 1200 °C and a nitrogen pressure of about 500 Torr in the chamber. The second harmonic radiation of a Nd:YAG laser with a pulse duration of 8 ns was focused on the surface of the target, providing an irradiation intensity of about 3 J cm^{-2}. The graphite target contained the admixture Ni + Co (1.2 at.%) used as a catalyst. Products of the thermal sputtering of graphite contained up to 50% single-walled nanotubes of 1.3 – 1.4 nm in diameter along with fullerenes and carbon particles. Most of the tubes were bound into bundles up to 30 nm in diameter. The electron energy loss spectroscopy measurements showed that the nanotubes practically do not contain nitrogen molecules. Nanotubes synthesized in a nitrogen atmosphere are similar in both yield and structural parameters to those for a helium atmosphere.

A natural way for developing the laser ablation method for CNT production is in the utilization of focused solar radiation [13, 40, 79]. The application of this approach is justified by the relatively low energy cost of solar radiation comparing to laser one. An experimental setup is presented schematically in Fig. 10b. A graphite target containing metal particles acting as a catalyst is inserted into an oven. The oven is heated with a power supply of 2 kW up to a temperature of about 1200 °C, and the target is irradiated with focused solar light. A mixture of powdered Ni and Co of 2 at.% each in content is used as a catalyst. As a buffer gas argon was utilized. The vaporization temperature of the irradiated surface ranges between 2900 – 3000 K. As the buffer gas pressure is increased, a rise in the yield of single-walled nanotubes is observed, which reaches a maximum at a pressure near 600 mbar. STM and TEM observations, and also Raman spectral measurements, show that nanotubes of 1.3 nm in average diameter are bound into bundles of 10 – 20 nm in diameter and several μm in length. These peculiarities of nanotubes make them similar to those formed in a cathode deposit through the electric arc synthesis.

Catalytic cracking of hydrocarbons. The most notable achievements in the technology of CNT production are based on performing the reaction of thermal decomposition of carbon-containing compounds in the presence of a metal catalyst. This approach, which is sometimes called the chemical vapor deposition (CVD) method, was used for the commercial production of thin carbon fibers well before the discovery of CNTs [80 – 83]. It was first applied to the production of CNTs in work [14], where the thermocatalytic decomposition of acetylene was performed in the presence of finely dispersed iron particles at a temperature of 700 °C. The layout of the process is illustrated in Fig. 11 [14, 70 – 73, 84, 85]. A catalyst, which is a finely dispersed metal powder, fills a ceramic crucible inserted into a quartz tube. This tube situated in an oven is kept at a temperature of 700 – 1000 °C and is blown with a mixture of a gaseous hydrocarbon and a buffer gas. The typical composition of the mixture is C_2H_2:N_2 with content in the ratio 1:10. The above-described procedure, which can take from several minutes up to several hours, results in the formation on the catalyst surface of

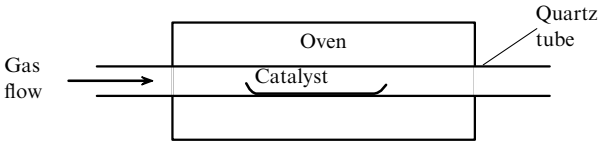

Figure 11. Schematic of a facility for CNT production by the chemical vapor deposition method [70 – 74].

elongated carbon filaments, metal particles enclosed in multilayer graphite shells and multilayer nanotubes up to several tens μm in length, more or of the order of 10 nm in inner diameter and up to 100 nm in outer diameter. The geometric parameters of the nanotubes formed are determined mainly by the conditions of the synthesis process (temperature, pressure and sort of the buffer gas), and also by the granule size and type of the catalyst.

The process of nanotube production, based on the application of chemical vapor deposition methods, has recently been intensively developed, relating to the elaboration of methods for large-scale growth of nanotubes on a patterned substrate. This offers a way to establish a mass industrial production of CNT-containing devices and facilities, including electron field emitters, which will be considered in detail below.

The growth of a large number of similar CNTs on a substrate of a large area is possible, if the parameters of the process are similar for all sections of the surface. In this case the major parameters are the size of catalyst particles and the state of sections of the substrate adjacent to those. Prominent advances in this direction have been made due to the development of methods for preparation of substrates having large surface area and high degree of the surface homogeneity. Besides, the development of methods for plating similar in size catalyst particles on a large-area surface is of importance.

A large body of research has resulted in the conclusion that the highest degree of homogeneity of CNTs grown with the CVD method is reached in the case of employing a porous substrate with the highest degree of homogeneity of pores. Then in the optimum situation the size of the pores fits that of relevant metal catalyst particles. In this case the diameter of the CNT growing from a catalyst particle is found to be close to the size of the particle and, correspondingly, to diameter of the relevant pore. If the depth of pores is quite large, and their surface density is quite high, nanotubes grow strictly perpendicularly to the substrate surface and are characterized by a high degree of homogeneity.

Therefore, the basic challenge in the mass production of CNTs relates to the preparation of the substrate surface and plating the catalyst material. The efforts of numerous research groups have been focused on the solution of this problem in the last few years. These efforts have resulted in several approaches. Thus, mesoporous silica plates doped with a metal catalyst [86], anodized alumina membranes [87, 88], microporous crystals $AlPO_4$ [89], etc. have been used successfully as a substrate.

The modern technology of substrate preparation can be inferred from work [90], where a mesoporous substrate was produced as a result of hydrolysis of tetraethoxylane $[(C_2H_5O)_4Si]$ in a water solution (0.1 – 1.5 M) of iron nitrate at a ratio $[(C_2H_5O)_4Si]$: ethanol:iron nitrate ranging between 1 : 4 : 10 and 1 : 4 : 14. Then concentrated hydrofluoric or hydrochloric acid (0.2 M) was added to the solution. The gel obtained in such a manner was dried over 7 days at 60 °C and then calcinated over 10 hours at 450 °C and a pressure of 0.1 Torr. This resulted in the formation of a porous substance with quite a high degree of homogeneity of pores which were filled with iron oxide nanoparticles. Then the iron oxide was reduced over 5 hours under a flow of hydrogen and nitrogen at a ratio $H_2 : N_2 = 1 : 10$, pressure of 0.23 bar, intensity of 100 – 150 ml min^{-1}, and a temperature of 550 °C, which resulted in the formation of iron particles at the bottom of the pores. The substrate produced was used for growth of CNTs, which was performed as a result of thermal decomposition of acetylene at 700 °C. STM observations showed that synthesis over 2 hours resulted in the formation of a layer of 50 mm in thickness, consisted of well-aligned rectilinear multiwalled nanotubes, on the substrate. A microscopic image of the nanotubes looks like thick tall grass. The nanotubes are separated from each other by about 100 nm on average and have an average outer diameter of about 30 nm. The inner diameter of the nanotubes is about 4 nm. A nanotube film is separated easily from the substrate and can be split in the direction of the axis of nanotubes. Carbon particles are observed in the interstitial space between nanotubes. X-ray analysis demonstrated that nanotube tips contain 98.76% of carbon and 1.09% of iron. Traces of silicon and oxygen (at the level of 0.2 wt. %) were found in some sections of tips.

Selective growth of CNTs on islands of $CoSi_2$ film deposited on a silicon substrate was demonstrated in work [91]. This work has become a notable step on the road to development of the CNT production technology compatible with the modern methods of industrial microelectronics. In the first stage of the process a Co film of 50 nm in thickness was deposited on a Si substrate as a result of electron beam irradiation of a Co target. Then the sample was annealed for 20 min at 800 °C in order to produce $CoSi_2$ film. The $CoSi_2$ surface was patterned using standard photolithography followed by ionic etching. After removing the photoresist, the height of the step, measured from the upper surface of $CoSi_2$ layer down to the naked Si substrate, comprised 160 nm. Therefore, the $Si/CoSi_2$ interface appears over the surface of a silicon substrate. The samples were inserted into a reactor heated up to 750 °C, which comprised a quartz tube through which nitrogen and acetylene were blown with rates of 300 and 40 $cm^3\,min^{-1}$, correspondingly. The reaction lasted for 60 min. After termination of the process, carbon structures were separated from the substrate through sonication in toluene and then, after drying, were subjected to STM observations. The growth of carbon tubular structures was observed only at the $Si/CoSi_2$ interface and was observed on neither Si nor $CoSi_2$ surfaces. The mean length of such longitudinal nanostructures is estimated as 500 nm. A 50 °C rise in the reactor temperature promotes the formation of nanotubes. The results of this experiment offer an opportunity for elaborating the technology of selective growth of CNTs on specific areas of the substrate surface with respect to the structure of a pattern.

As is seen, the procedure of producing well-aligned nanotubes on a large area is rather complicated and involves several stages. The most technologically difficult of the latter is the process of substrate preparation. An appropriate attempt at considerable simplification of this procedure was performed recently in work [92], where the thermocatalytic decomposition of acetylene or CO resulted in the production of both multiwalled and single-walled nanotubes. In doing so iron carried by iron pentacarbonil $Fe(CO)_5$ was used as a catalyst. Single-walled CNTs were synthesized by inserting CO with an admixture of $Fe(CO)_5$ and (in some cases) H_2 through a water-cooled injector into an oven heated up to 1100 °C. Thermal dissociation of $Fe(CO)_5$ was accompanied by the formation of iron clusters which served as a catalyst for nanotube growth. The process resulted in the formation of single-walled nanotubes and iron particles, enclosed into multilayer graphite shells, on the surface of

the ceramic crucible. The addition of some quantity of H_2 to the $CO/Fe(CO)_5$ mixture increased the yield of single-walled nanotubes. Since the commercial CO used in the experiment contains some admixture of $Fe(CO)_5$, there was no necessity for special addition of $Fe(CO)_5$. Vertically aligned multiwalled nanotubes were produced through the thermocatalytic decomposition of acetylene on a silicon substrate covered with iron particles at a temperature of 750 °C in the presence of Ar. The iron particles were formed as a result of decomposition of $Fe(CO)_5$ at 200 °C.

Experiments devoted to nanotube growth on silicon plates should be noted as an important stage on the road to the development of a technology for industrial mass production of CNTs. Indeed, silicon is the most widely used material in microelectronics. The best results were reached using specially prepared porous silicon, the structure of which promotes the growth of CNTs [93]. Samples of porous silicon 5 cm in diameter with resistivity ranging between 0.008 and 0.018 Ω cm were produced through the electrochemical etching of $n^+ - Si(100)$ plates highly doped with phosphorus. The etching lasted for 5 min in a teflon cell with the employment of a platinum cathode, halogen lamp and 1:1 mixture of 50% water solution of hydrofluoric acid and ethanol. The current density of anodization was kept at the level of 10 mA cm^{-2}. As a result of the etching, a macroporous layer of the substrate, which was characterized by pores of a submicron size, became coated with a nanoporous layer with a pore size of order 3 nm. Aside from the porous silicon plates, smooth p-type silicon substrates produced through doping with boron and having resistivity within the region 5–10 Ω cm were used for growth of CNTs. Substrates of both types were plated with a Fe film of 5 nm in thickness, using electron beam deposition through shadow masks having square holes 10–250 μm in size and separated by 50–200 μm. The substrates produced in such a manner were annealed over several hours at 300 °C. Then they were inserted into a cylindrical quartz crucible sealed off from one end, which was situated in the central part of a quartz tube 5 cm in diameter. The synthesis of nanotubes was performed over 15–60 min at a temperature of 700 °C in a cylindrical oven with the quartz tube, through which a mixture of heated Ar and acetylene was blown at a rate of 1000 cm^3 min^{-1}

The above-described procedure resulted in the formation on the substrate surface of a matrix consisting of vertically aligned regularly arranged bulks of multiwalled nanotubes. STM images of this matrix, obtained for two types of the silicon substrate, are shown in Fig. 12. As is seen, the size of each bulk exactly fits the square hole filled with Fe film. All the nanotubes observed are of 16 nm in diameter. Nanotube matrices grown on porous silicon substrates are characterized by a more perfect structure compared to those grown on smooth silicon. In this latter case some of the highest nanotube bulks are arranged not vertically, but at some angle relative to the surface of the substrate. Besides, the nanotubes produced in such a manner are distinguished by a larger diameter, higher defect density and also the presence of catalyst particles over some bulks. It is interesting to note that after removing the nanotube bulks the substrate surface retains its ability to grow aligned nanotubes as a result of chemical deposition of ethylene. Therefore, the mechanism of growth of aligned nanotubes in the conditions under consideration relates to processes running on the substrate surface, but not on nanotube tips. The emission properties of the produced nanotube matrices will be described in subsequent sections of the article.

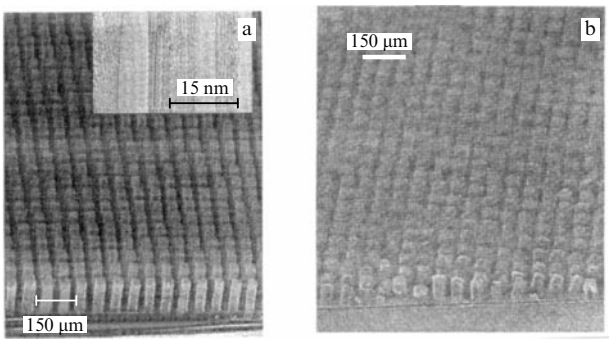

Figure 12. SEM images of CNT matrices grown on the substrates of porous (a) and smooth (b) silicon [93].

One of the important peculiarities of the method of CNT production based on the thermocatalytic decomposition of hydrocarbons relates to the possibility of controlling the geometric parameters of nanotubes produced by means of variation of the process parameters. This possibility was shown, in particular, by the authors of work [94], where various transition metals (Co, V, Mo, Fe) and their alloys were used as catalysts. A catalyst in the form of a 5% solution of transition metal salts was applied to a substrate (zeolite NaY or corundum Al_2O_3). The substrate was inserted into a quartz crucible, which was kept at a temperature of 700 °C and was blown with a mixture of acetylene with nitrogen (1:10) for 1 hour at a rate of 330 ml min^{-1}. The deposit obtained was observed by means of TEM of low and high resolution. Table 1 gives the yield of multiwalled nanotubes in the deposit (in percentages relative to the catalyst mass), which were obtained using various catalysts and substrates. As is seen, the combination of two metals and substrate material has a synergy effect on both the quantity and quality of the deposit produced. The best results from the viewpoint of nanotube yield are reached through the employment of Co – V or Co – Fe alloys, while the best quality of nanotubes is reached when using Co – Mo.

Table 1. Deposit yield (%) obtained using various catalysts and substrate materials [94] (X = V, Mo or Fe).

Catalyst (substrate)	Deposit yield (%) for different metal ratios Co : X (wt. %) in the catalysts				
	0 : 5	1 : 4	2.5 : 2.5	4 : 1	5 : 0
Co – V (zeolite)	0	46	116	55	25
Co – V (corund)	0	6	127	18	2
Co – Mo (zeolite)	0	—	30	—	25
Co – Mo (corund)	0	—	25	—	2
Co –Fe (zeolite)	48	38	120	144	25
Co – Fe (corund)	11	75	157	8	2

Table 2 presents the average outer diameter of multiwalled nanotubes produced with various bimetallic catalysts and substrates. The content of a bimetallic catalyst is as follows: Co : X = 2.5 : 2.5 wt.%. The observed dependence of the mean diameter of nanotubes on the content of the catalyst and the type of substrate used points to the possibility of synthesis of multiwalled nanotubes with a desirable diameter distribution.

Table 2. Mean outer diameter of multiwalled nanotubes produced using various substrates and bimetallic catalysts [94].

Catalyst	Co – V	Co – V	Co – Mo	Co – Mo	Co – Fe	Co – Fe
Substrate	zeolite	corund	zeolite	corund	zeolite	corund
Mean diameter, nm	7.5	10.3	10.0	10.0	17.8	12.8

Methods of purification of CNTs. As already noted, the products of any thermochemical transformation of graphite contain not only nanotubes but also a considerable quantity of admixtures. Among these are firstly nanometer-sized particles of graphite or amorphous carbon and also, in the case of using metal catalysts, metal particles which are typically enclosed in multilayer graphite shells. Specially elaborated procedures are employed for enhancement of the nanotube content in a raw material. The effectiveness of them depends on the method implemented for producing the material. These procedures combine well-known methods of mechanical processing (filtration, sonication, and centrifugation) with chemical and thermochemical approaches based on the employment of chemically active substances (acids, hydrogen peroxide, etc.) and also on heating the material in the presence of air or oxygen. Since carbon nanotubes have no free bonds, their chemical stability considerably exceeds that of graphite and metal particles. Therefore, the above-listed procedures result in a notable decrease of content of impurity particles, so that in appropriate conditions one can obtain a material containing practically pure nanotubes.

Thus, in work [95] single-walled nanotubes produced through the laser ablation of graphite were washed in 2 – 3 M concentrated nitric acid, followed by the centrifugation. The rest of the acid was removed by means of deionized water and also of NaOH solution (pH = 11), whereupon the material was inserted into 3 : 1 mixture of 98% sulphuric acid with 70% hydrochloric acid and stirred for 20 – 30 min at a temperature of 70 °C. Finally, the rest of the admixtures were removed with a 4 : 1 mixture of 98% sulphuric acid and 30% hydrogen peroxide. TEM observations showed that practically no admixtures present in the obtained samples of single-walled nanotubes.

Unlike fullerene molecules, CNTs are virtually insoluble in organic solvents. This hinders their purification by methods and approaches based on ideas of liquid chromatography (see, e.g., Refs [96, 97]). However, experiments have already been attempted on purification and size separation of nanotubes, where a nanotube-containing suspension is passed through a porous material. This method, called *size exclusion chromatography*, was first realized in work [98], where a porous glass was utilized as a stationary phase. The experiments were performed with both the material containing multiwalled nanotubes (10 mg), which was produced through the standard electric arc method, and that containing single-walled nanotubes (1 mg), which in turn was produced through the laser ablation method in the presence of a Ni/Y catalyst. The material was added to 2 ml of 1% water solution of sodium dodecylsulphate (SDS), where it was ultrasonicated for 5 min. After a settling time of 15 min, the suspension separated into two fractions — a black supernatant and a dense deposit. The supernatant, which is stable for several days, was subjected to the chromatographic treatment.

The material containing multiwalled nanotubes was separated by means of two successive columns. The first one was destined for removal of the smallest size particles and fullerenes. This column of 7 cm $\times$ 2 cm^2 in active volume was filled with a porous glass having a mean pore size of 140 nm. The column was loaded with 1.5 ml of supernant and washed with 0.25% water solution of SDS (pH = 7). The flow rate measured 9 ml h^{-1}. Within 1.7 hrs of the beginning of the flow, two fractions of 6 ml in volume were collected. The first was concentrated to 1.5 ml by the addition of 100 mg polyacrylamide adsorbent gel followed by continuous shaking for 30 min. Then the concentrated first fraction was loaded into the second column of 33 cm $\times$ 1 cm^2 in volume filled with a porous glass with an average pore size of 300 nm, which was washed with a flow rate of 5 ml min^{-1}. Within 3 h of the onset of the flow, 8 fractions of 1.5 ml in volume were collected. Only the second column was involved in the procedure of purification of single-walled nanotubes. The concentration of SDS solution was 1%. The fractions produced were subjected to centrifugation.

As follows from the results of investigations, the dispersed material containing CNTs passes almost fully through the column. The exception is large-sized particles which comprise about 10% of the mass of the material and precipitate in the upper section of the column. TEM and STM observations show that the fractions extracted after washing the second column differ considerably from each other in their composition. Thus, the first fraction contains aggregates of CNTs and other carbon particles, whereas fractions 7 and 8 contain mainly spherical particles and some quantity of multiwalled nanotubes less than 0.1 μm in length. Fractions 2 – 6 contain individual multiwalled nanotubes and also some quantity of spherical particles whose content increases with rising fraction number. Similar composition of the fractions is also observed in the case of single-walled nanotubes. However, in this case the centrifugation of chromatographically separated fractions resulted in both removal of most of the CNTs with attached catalyst particles, and a lowering of the total yield of CNTs. Measurements showed that the purified material contains about 50% of single-walled nanotubes, in part isolated and in part bound into bundles. The measured distributions of single-walled nanotubes over the length have different forms for various fractions. Thus, the mean nanotube length in fraction 3 is of 1 μm, whereas that in fraction 5 is 0.6 μm. A similar conclusion applies to multiwalled nanotubes. So one can believe that chromatographic size separation of CNTs has been performed.

The chromatography method for separation of nanotubes has been further developed in successive works [99, 100], where the raw material containing single-walled nanotubes was produced through the standard electric arc method. The purification process involves 3 stages. Initially the raw material is treated for 3 h in 65% nitric acid (100 mg of raw material per 150 ml of acid). This results in about 20% loss in the material mass. Then the material is ultrasonicated for 1 min. This causes a decrease in the size of nanoparticles and, to a lesser degree, shortening of bundles and nanotubes. The last stage, which is the most important one, involves the chromatographic separation of single-walled nanotubes and nanoparticles. Potassium polyacrylat flooded with distilled water is utilized as a stationary phase. In order to precipitate the process, the output of the column is connected to a vacuum pump. Then the polymer particles are contract like a sponge, until the extraction terminates. Single-walled

nanotubes move in a space between polymer particles and are extracted with a yield of about 40% as the first fraction. The rest of the material also contains single-walled nanotubes which can be extracted in successive stages, but with a lower yield. The majority of by-products remain inside the stationary phase. The purification process was monitored by Raman spectrometry, so that the relative yield of single-walled CNTs was estimated by the intensity ratio between the G-line (1580 cm^{-1}) belonging to single-walled nanotubes and the D-line (1350 cm^{-1}) inherent to carbon particles. The obtained samples of purified nanotubes were used in subsequent experiments devoted to functionalization of CNTs with the carboxyl acid group.

Work [101] presents a detailed description of a multistage procedure of purifying the single-walled nanotubes, including a close control of the material composition in all stages of the procedure. This allows an understanding of the role of each of the stages in all the procedure, which offers a possibility for the optimization of the process and further development of methods for nanotube purification. The initial material was produced through the laser ablation method. It contained single-walled nanotubes bound into bundles of about 20 individual tubes, and also particles of amorphous carbon and metal (Fe, Ni) from 10 up to 100 nm in size, enclosed in the graphite shell. 100 mg of this material was inserted into a cap filled with distilled water and heated up to 100 °C while stirring. The interaction of graphite shells with water molecules destroys the bonds of nanotubes with each other and also with particles of amorphous carbon and metal. Then the sample was subjected to a filtration and a long drying at 80 °C. The resulting soot was warmed for 45 min at 700 °C, which was followed by treatment in hydrochloric acid (6 M) at 100 °C.

The sample was studied through the X-ray diffraction and transmission electron microscopy methods at each of the purification stages. These studies showed that the hot water treatment results in the removal of a considerable quantity of amorphous carbon and destroys bonds between nanotubes constituting bundles. Heating samples up to 700 °C in air causes oxidation of metals up to NiO and Fe_2O_3, which is followed by a loss of 40 wt.% of the sample. The last stage of purification, involving the acid treatment of samples, results in the dissolution of all the oxides.

One of the most effective approaches to purification of nanotubes is based on heating the material containing nanotubes in the presence of oxygen or air. This approach is sometimes called thermal gravimetry and allows the removal of practically all metal particles, whose oxidation temperature is considerably lower than that for CNTs, as well as finely dispersed amorphous carbon which is more prone to oxidation in comparison with nanotubes due to the presence of free bonds. The approach mentioned was demonstrated, in particular, in work [102], where it was used for purification of a cloth-like material containing single-walled nanotubes. The sample was produced in a dc arc discharge. A hole of 3 mm in diameter and 70 mm in length was drilled in a cylindrical graphite anode of 6 mm in diameter and 300 mm in length. This hole was filled with a 3 : 10 mixture of graphite with either powdered YNi_2 alloy or powdered blend of CaC_2 and Ni. A graphite rod of 10 mm in diameter with a sharpened end facing the anode was utilized as a cathode. The arc was burnt at a current of 40 A and a pressure of 700 Torr. The interelectrode gap was kept at a level of 5 mm. When the anode rod had burnt for 10 cm, about 5 g of cloth-like material containing single-walled CNTs was extracted from camera walls. This material was subjected to thermal gravimetry analysis (TGA), which consisted in heating the sample at the rate of 10 °C min^{-1} under an air flow of 70 cm^3 min^{-1} and monitoring the weight of the sample. As follows from the thermal gravimetry data, a notable loss in weight of the sample due to oxidation is observed at temperatures above 200 °. The temperature dependence of the rate of loss in weight therewith shows four peaks which are attributed to the maximum in the oxidation rate of amorphous carbon (381 °C), single-walled nanotubes (471 °C), fullerene molecules (568 °C), and nano-sized carbon particles (635 °C). These data imply the possibility of effective usage of thermal gravimetry treatment of a material containing nanotubes not only for the analysis of its composition but also for purification from major admixtures. The authors recommended 350 °C as the value of the treatment temperature. This treatment in combination with the utilization of fine filters allows the admixture content to be lowered to 10%.

The above-described approach has been further developed in succeeding works [103, 104], which were also performed with the participation of the discoverer of nanotubes S Iijima. In these works, the authors tried to overcome the main difficulty of using the thermal gravimetry method of CNT purification, which is the proximity of the inflammation temperature for single-walled nanotubes and amorphous graphite. This proximity causes a notable loss in nanotube material during purification. In the above-cited works [103, 104], the possibility of a predominant oxidation of amorphous carbon particles by means of ultradispersed gold and a cation surfactant has been demonstrated and optimum conditions for such a process have been stated.

Single-walled nanotubes were produced by the laser ablation method using the second harmonic of a Nd : YAG laser with a wavelength of 532 nm, pulse duration of 6 – 7 ns, repeating frequency of 10 Hz, and incident radiation intensity of 25 W cm^{-2}. The camera was 60 cm in length and 3.6 cm in diameter. The target was produced by co-pressing powdered graphite, Ni and Co. The content of each of the metal was 0.3 at.%. The irradiation of a target for 20 min resulted in the formation of about 20 mg of web-like nanotubes near the camera outlet. Banzalconium chloride (BAC) was utilized as a surfactant. Experiments on the optimization of the gold particle content were performed with 14 ml water suspension containing 4 mg nanotubes, ultradispersed gold particles of 20 nm in diameter at a concentration varied between 0 and 1.2 at.%, and BAC at a concentration of 10 g l^{-1}. The concentration of BAC was optimized at a gold particles concentration at the level of 0.6 at.%. After mixing and sonication, the suspension was dried at 180 °C. Then the material containing nanotubes and particles of graphite and carbon was subjected to thermal gravimetry processing, which consisted in heating it up to 1000 °C in argon with an admixture of 1% oxygen at the rate of 10 °C per minute. In doing so the weight of the sample was monitored continuously. Thermal gravimetry curves of nonpurified nanotubes show two broad peaks at 600 and 800 ° C, and a shoulder at 450 °C. Insertion of gold particles into the suspension results in a displacement of the features in the curve to a low-temperature region, so that the peak is observed at 550 °C, and two shoulders at 400 and 680 °C. Inserting BAC (without gold) and its removing at the subsequent vaporization results in the appearance of peaks at 550, 700 and 850 °C. Inserting

both BAC and gold particles into the suspension causes a displacement of these peaks to 480, 650 and 830 °C, respectively. These data demonstrate the influence of gold particles and BAC on the inflammation temperature of carbon materials.

SEM and Raman spectroscopy observations performed at various stages of the thermal gravimetry procedure show that the quantity of amorphous carbon is not decreased on heating up to 350 °C. Heating up to 550 °C results in a sharp decrease of this quantity, while the number of nanotubes does not change notably. Heating up to 730 °C is followed by a notable decrease in the number of bundles of single-walled nanotubes and the appearance of spherical particles of about 50 nm in diameter. One can conclude that amorphous graphite is burnt mainly over the temperature region 300 – 550 °C, while the rest is burnt at a temperature exceeding 730 °C. Investigations imply that the optimum concentration of gold particles is 0.6 at.%. The optimum concentration of the BAC water solution is estimated at the level of 7 g l^{-1}. The authors attribute the role of BAC to a homogenization of graphite particles, i.e. to a narrowing of their size distribution function.

4. Electronic properties of carbon nanotubes

Interconnection of structural and electronic characteristics of CNTs. One of the important peculiarities of CNTs is the interconnection between their structural and electronic characteristics. This interconnection shows up firstly in the dependence of the electronic structure of a nanotube on its chirality. This dependence follows from the results of numerous theoretical evaluations of density of occupied states for graphite nanotubes [105 – 112] (see also the methodically quite interesting series of papers [113 – 115]). These states are formed as a result of delocalization of 2s- and 2p-electrons of the carbon atom, so that the 2s-electrons at hybridization fill energy regions below and above the Fermi level, while the 2p-electrons fill a region near the Fermi level. Calculations show that a change in chirality and correspondingly nanotube radius also changes the energy gap width, which decreases monotonically as the radius rises.

It is convenient to use the index $k = m - 2n$ ($m > 2n$) instead of the above-introduced indices (m, n) as a factor determining the influence of the chirality on electron characteristics of nanotubes of a prescribed diameter [35]. Thus, a nanotube with $k = 0$, corresponding to the chirality angle $\theta = \pi/6$, possesses metallic conductivity; $k = 3(q + 1)$ relates to a narrow gap semiconductor, and $k = 3q + 1$ and $k = 3q + 2$ ($q = 0, 1, 2, \ldots$) correspond to a semiconductor with a moderate energy gap width.

Quantitative relations between the chirality indices of an ideal single-walled nanotube, its radius and energy gap width can be stated only on the basis of model calculations using strongly simplifying assumptions. For these reason the calculated results obtained by various authors [105 – 112, 116] differ from one another in some details. However, these data feature common tendencies. The tendencies are illustrated in Fig. 13a, where the dependences of the energy gap width ε_g on the reduced radius $R_d = R/d_0$ of a long single-walled nanotube, calculated in work [116] for various magnitudes of the chirality index of a long single-walled nanotube, are shown. Here, R is the nanotube radius, $d_0 \approx 0.14$ is the interatomic distance on the graphite plane, and the energy gap width ε_g is expressed in units of the interaction energy $\varepsilon_{pp\pi}$ of two p-electrons belonging to neighboring carbon atoms in the graphite lattice and resulting in the formation of a π-bond. This energy is known with a rather limited accuracy, so that the data given have a qualitative character. The solid line in the figure corresponds to the dependence $\varepsilon_g = 1/R_d$, which has been stated by the authors of Ref. [107] using a simplified approach neglecting the dependence of the interaction energy of p-electrons on the nanotube radius. The inversely proportional dependence of the energy gap width on the nanotube radius, as well as the statement about the metallic character of electron conduction in nanotubes with $k = 0$ hold in all the model calculations performed up to now.

The above-stated dependence was derived experimentally in works [113 – 115], where current – voltage characteristics of single-walled CNTs of various diameter and chirality were measured in vacuum at $T = 77$ K using SEM. The interrelation between structural and electronic characteristics of

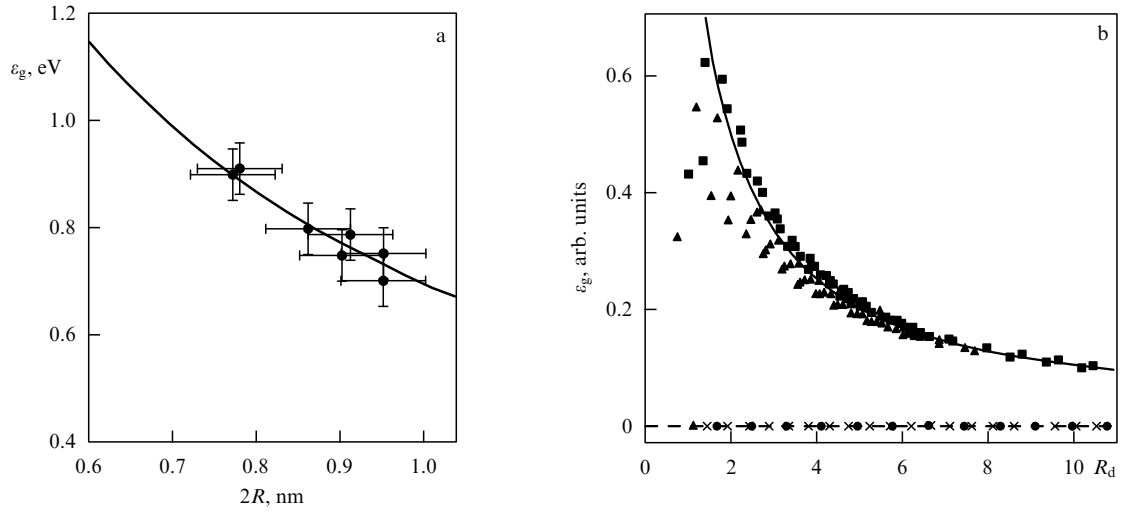

Figure 13. Dependences of the energy gap width on the nanotube radius, calculated (a) [116] and measured (b) [115] for nanotubes of various chiralities. $R_d = R/d_0$ is the dimensionless radius of a nanotube, expressed in units of separation between the neighboring carbon atoms in the graphite lattice ($d_0 = 0.142$ nm); the solid lines trace the inversely proportional dependence $\varepsilon_g \sim 1/R$.

CNTs was verified in experiment. The structure of an individual nanotube situated on the surface of a bundle was studied with an atomic resolution which allowed determination of its diameter as well as the chirality angle α and indices (m, n). Thus were measured the magnitudes $d = 1.00 \pm 0.05$ nm and $\alpha = -8.0 \pm 0.5^\circ$ for one of the nanotubes studied. This may correspond to the chirality indices either $(11, 2)$ ($d = 0.95$ nm and $\alpha = -8.2^\circ$) or $(12, 2)$ ($d = 1.03$ nm and $\alpha = -7.6^\circ$). For another nanotube studied one has $d = 1.08 \pm 0.05$ nm and $\alpha = -11.0 \pm 0.5^\circ$, which is attributed to indices $(12, 3)$ corresponding to $d = 1.08$ nm and $\alpha = -10.9^\circ$. The current – voltage characteristics of these nanotubes, measured by means of STM, imply the metallic conductivity of both. Since the quantity $(2n + m)/3$ for such a tube should be an integer, which is the case for the second nanotube, one can conclude that the chirality indices of the second nanotube are $(11, 2)$. A number of semiconductive nanotubes were observed in this experiment along with metallic ones. Figure 13b presents the dependence of the energy gap width of a semiconductive CNT on its diameter, evaluated on the basis of measured current – voltage characteristics of individual single-walled nanotubes of varying diameter [115]. These data are the result of averaging over nanotubes of various chiralities. As is seen, the dependence measured agrees quite well with the inversely proportional relationship $\varepsilon_g \sim 1/R_d$, which follows from a simplified model approach. The findings of the work cited imply a wide variety of nanotube structures which are formed as a result of laser ablation of graphite.

Conductivity of nanotubes. Good emission characteristics of CNTs are caused, on the one hand, by their unique structure and, on the other hand, by their high electron conductivity. Considering the mechanisms of conductivity and analyzing a large body of relevant experimental data, one should discriminate the conductivity of individual nanotubes (single-walled and multiwalled) and that of a material consisting of such tubes as elements. Since a CNT is a graphite surface rolled in a cylinder, one can expect that the characteristic magnitude of its conductivity in the longitudinal direction is comparable with that along the graphite surface. However, as follows from the analysis of the large set of experimental data obtained up to now, even the measured values of conductivity of individual single-walled nanotubes, obtained by various groups, can differ from each other by several orders of magnitude. This stems from the distinctions in structures of single-walled nanotubes and, in particular, in their chiralities. Besides, surface defects of nanotubes can have some impact on the conductivity. This is caused by not only possible departure of the structure from the ideal hexagonal one, but the presence of added radicals (OH, CO, etc.) as well, changing the position of both valence and conduction bands. Thus, nanotubes produced by various experimental methods, using diverse experimental facilities, are characterized by differing magnitudes of conductivity. Moreover, even nanotubes produced with a common experimental setup, but extracted from various surface regions of an experimental chamber, can have distinctive conductivities. One can say the same about the temperature dependence of the nanotube conductivity which usually provides information concerning the mechanism of electron conduction in a material. Various characters of behavior and even signs of this dependence were observed for both single-walled and multiwalled nanotubes.

The conductivity of individual CNTs is determined mainly by their geometry and the presence of defects. By contrast, that of the material consisting of CNTs is appreciably dependent on the quality of the contact between neighboring nanotubes, and on the presence and composition of admixtures as well. Thus, both the absolute values and the character of the temperature dependence of the conductivity of such materials are determined by not only the production method used but also the degree of their purification.

Direct measurement of the conductivity of individual nanotubes is a rather hard technical problem. On the one hand, this is related to the tiny size of nanotubes, which hinders the performance of reliable measurements. On the other hand, it is caused by the very low resistivity of an individual nanotube, which is frequently less than that of the lead-in contacts. This brings the necessity of designing such a measuring scheme, which excludes fully or partly the role of the contacts. Nevertheless, in spite of these difficulties, a large number of papers have been published recently, reporting such measurements with the use of modern methods of manipulating nanometer objects.

Detailed measurements of the conductance of individual single-walled nanotubes produced as a result of laser sputtering of graphite in the presence of a catalyst were performed in work [117] published recently. Small amount of the material produced after ultrasonic dispersion was applied to the surface of an SiO_2/Si substrate covered with a lattice of platinum electrodes no higher than 1 nm in height. The conductance of both an individual nanotube and internanotube contact were measured by means of an atomic field microscope (AFM). The main result of these measurements was the high sensitivity of the conductance of a nanotube to the degree of its bending. The tip of the microscope was pressed to a rectangular nanotube, which resulted in either its lateral bending (the angle is close to 105°) or its lateral angular contact with a neighboring nanotube. This measurement procedure permits discrimination between the contact resistance and that of the nanotube itself. In accordance with these measurements, the room-temperature conductance of a rectangular section of a single-walled nanotube, not subjected to external pressure, is about 100 μS, which corresponds to a resistance of 10 kΩ. To an order of magnitude this is comparable with the value of the unit of quantized conductance $4e^2/h = 154$ μS, which corresponds to the ballistic mechanism of charge transport, and considerably exceeds the contact conductance estimated as 65 nS. Bending the nanotube at an angle of about 105° results in about a 100 times decrease in its conductance which reaches approximately 1 μS. Thus, the bending of a nanotube drastically changes its conductivity.

The above-described property of nanotubes can be used as the basis of a new class of superdiminutive transducers of a mechanical signal into an electrical one, and conversely. A time-dependent mechanical force acts on a single-walled nanotube connected into a circuit, which leads to its bending and, correspondingly, a change in conductivity. This leads to a change in the voltage drop over the relevant section of the nanotube, which, after a standard amplification procedure, can be used as a sensing element of tiny mechanical displacements and the basis for a miniature microphone as well.

Figure 14 presents the temperature dependences of the conductance of a bent nanotube section, measured by two-contact and four-contact methods. In the temperature range above 100 K, these dependences are well approximated by a

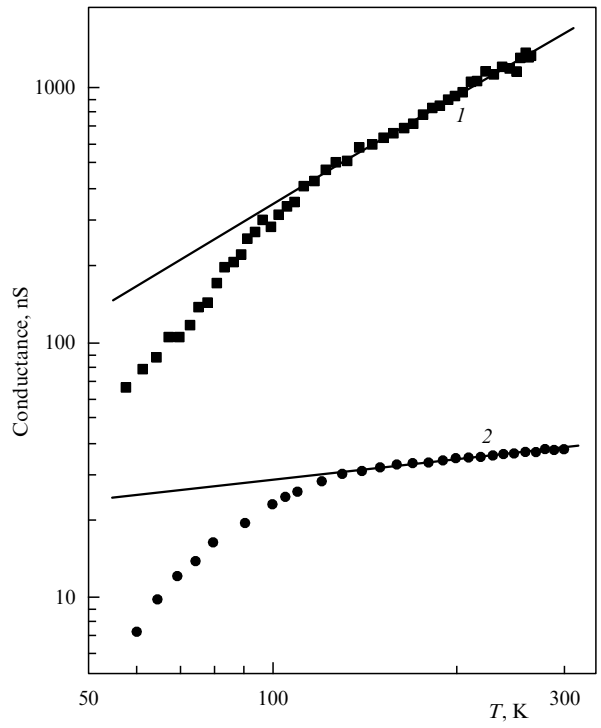

Figure 14. Temperature dependence of the conductance of an individual single-walled nanotube, measured by two-contact (*1*) and four-contact (*2*) methods [117]. The solid lines correspond to power dependences $G \sim T^{\alpha}$, where $\alpha = 1.4$ (*1*), and $\alpha = 0.26$ (*2*).

power law $G \sim T^{\alpha}$, where the fitting parameter $\alpha = 0.26$ in the case of two-contact measurements, and $\alpha = 1.4$ in the case of four-contact measuring circuit. The four-contact measured data therewith correspond more closely to the conductance of a bent section proper. The magnitude of the power index of the relevant temperature dependence implies the tunnel mechanism of charge transfer through the bent section. So the data obtained show the possibility of artificial creation of a tunneling junction in an individual nanotube through its bending. The contact between two crossed nanotubes is characterized by a room-temperature conductance of 80 nS. Since this magnitude is much less than the quantized conductance, one can conclude that the crossing point acts as a tunneling junction.

The resistance of an individual nanotube and a contact resistance at a boundary with current feeders were measured in work [118]. In doing so, the tip of the AFM was used as a local voltmeter. A nanotube surface is scanned by means of an AFM tip under an applied voltage. The electrostatic force acting between the tip and sample is measured by two methods. In accordance with the first, the AFM tip is out of contact with a cantilever which is subjected to self-vibrations near the surface of the sample. The self-vibration frequency of the cantilever depends, in particular, on the voltage at the relevant point of the sample. In accordance with the second method, the cantilever is subjected to an applied alternating voltage, the frequency of which is equal to that of self-vibrations. In this case the useful signal is the vibration amplitude which turns out to be proportional to the voltage inside the sample. The signal was calibrated by means of a fixed constant voltage applied to the sample. In such a manner the potential distribution over the nanotube length was measured. The linear shape of this dependence indicates the possibility of using the method described to measure the resistance of nanotubes but not contacts. The resistivity of a multiwalled nanotube of 9 nm in diameter was measured as 10 kΩ μm^{-1}. This is in an agreement with preceding data [119, 120]. The contact resistance is evaluated by extraction of the proper nanotube resistance from the total one. This procedure results in the following values for the resistance of the left and right contact, correspondingly: 6 ± 2 and 3 ± 2 kΩ.

Similar measurements provide an estimate for the proper resistance of a metal-conductive single-walled nanotube as 3 kΩ. These measurements show that the resistance of a metal-conductive single-walled CNT is much less than those of contacts, which are estimated as 28 and 12 kΩ, correspondingly. The obtained magnitude of conductance of a single-walled nanotube suggests a ballistic mechanism of charge transfer, in accordance with which electrons pass the length of a nanotube > 1 μm without scattering. This conclusion is in a qualitative agreement with the preceding measured data [121] obtained by the two-contact method.

A semiconductive single-walled nanotube shows a much higher resistance (about 60 MΩ). The measured data therewith exhibit sensitivity to the point of application of the tip. The analysis of measured data indicates that the resistance of semiconductive single-walled nanotubes is determined by barriers positioned along the length of a nanotube and spaced 100 nm apart. The origin of these remains to be clarified.

The magnitude of contact resistance between a nanotube and current feeders deserves special attention. The studies performed recently have shown a decisive dependence of this parameter on the material of current feeders [122]. As the object of investigation the bundles of single-walled nanotubes were used, which were deposited on a silicon substrate covered with an oxide layer of 300 nm thickness after the standard purification procedure. The electrode matrix was fabricated by means of electron-beam lithography, for which purpose the substrate was covered with two layers of a resist on the basis of polymethyl metacrylate. Electrical measurements were performed in a He atmosphere. The current – voltage characteristics of CNT bundles in contact with Au, AuPd, Al and Co were measured at both $T = 4$ K and room temperature. The measurements show that the contact resistance of bundles of single-walled CNTs with Au and AuPd amounts to several tens of kΩ, which is comparable with the magnitude of $h/e^2 = 25.9$ kΩ and suggests the ballistic conduction mechanism. The contact with Al is practically not conductive, whereas the contact with Co has a resistance of hundreds of kΩ. The findings described point to the important role of adhesion between the nanotube material and current feeders in providing the electrical contact.

While the conductance of single-walled nanotubes is in satisfactory agreement with the ballistic mechanism of charge transfer, the description of that of multiwalled nanotubes requires the application of more complicated models. On the one hand, the phenomenon of quantized conductance observed in some experiments (see, for instance, Ref. [123]) is attributed to the ballistic conductance of the external shell. On the other hand, a weak localization of carriers and the occurrence of Aharonov – Bohm oscillations in the magnetoresistance at low temperatures imply that the coherence length corresponds to the diffusive charge transport involving more than only one external shell [118].

The conduction mechanism of multiwalled nanotubes was clarified somewhat as a result of the performance of experiment [124], where the conductance was measured by the four-contact method. The nanotubes grown by the standard electric arc method were ultrasonicated and centrifuged in dichloroethane for the removal of admixtures. The suspension produced was applied over a silicon substrate, which was previously covered with a lattice of gold electrodes. The electric conductance of individual multiwalled nanotubes with diameters ranging between 3 and 40 nm was measured at various mutual arrangements of nanotubes and contacts. The proper contact resistances ranged between 1 and 10 kΩ. The interelectrode gap L was varied between 100 and 400 nm, which provided the measurement of the resistance of the nanotube along its length. The measurements showed that the dependence of the resistance R of a nanotube on its length and diameter D was in good agreement with the relationship

$$R = \frac{\rho L}{\pi D},$$

where $\rho \approx 700$ Ω cm is the resistivity. Such a behavior of the resistance suggests a nonballistic character of the charge transport. Therefore one can conclude that a multilayer nanotube is a classic two-dimensional conductor of L in length and of D in diameter.

However, these data can also be treated in terms of quantum quasi-one-dimensional conduction. Indeed, since the density of electronic states at the Fermi level $N(E_F) \sim D^{-1}$, the mean free path of an electron in relation to the elastic scattering $l_e \sim N^{-1}(E_F) \sim D$. Because the resistance is inversely proportional to the free path, it should also be inversely proportional to the nanotube diameter. This is in agreement with a conduction model, in accordance with which an outer electrode in contact with the external shell of a nanotube also provides contact between the external and an (at least one) internal shell. This results in the formation of a branched network which determines the current – voltage characteristic observed in experiment.

5. Electron field emission of carbon nanotubes

Electron field emission. The phenomenon of electron field emission (EFE) occurs as a result of the action of an external electric field on a grounded conductor. This action provides the conduction electrons which are originally in a rectangular potential well, with the possibility for quantum tunneling escape out of the conductor. At zero electric field strength there is a rectangular potential barrier for electrons of the metal, the height of which is determined as the work function φ. So that only such electrons are able to leave the metal whose energy exceeds the magnitude of φ. Since this magnitude usually amounts to several electron-volts, which is 1 – 2 orders of magnitude as large as the room temperature, the number of such electrons is practically negligible. The application of an external electric field results in a decrease of the barrier height by $\Delta\varphi$, the magnitude of which rises as the electric field strength is increased. Besides, a tunneling electron transition through the barrier has been made possible, so that the barrier width is lowered sharply as the electric field strength rises. This results in the occurrence of electron emission, the current being a sharply rising function of the applied voltage.

A simple model approach (see, e.g., Ref. [125]) to a quasi-classic description of the EFE phenomenon treats it as a process of electron tunneling through the barrier formed by an ionic metal lattice and an external electric field. This approach suggests spatial homogeneity of the electron energy distribution function in a metal. In this case the above-mentioned distribution is described by the Fermi – Dirac function

$$f(\varepsilon, T) = \frac{1}{1 + \exp(\varepsilon - E_F)/T}, \tag{4}$$

where ε is the electron energy, T is the temperature, and E_F is the Fermi energy. In the simplest case of a flat metallic surface oriented transversely to the vector of the electric field strength, this relation is followed by the expression connecting the EFE current density J and the electric field strength E at a boundary of the conductor:

$$J = C_1 E^2 \exp\left(-\frac{C_2}{E}\right). \tag{5}$$

Here the following notation is used

$$C_1 = \frac{e^3}{8\pi h\, t^2(y)\, \varphi}, \quad C_2 = \frac{8\pi\sqrt{2m}}{3he}\, \varphi^{3/2}\, \vartheta(y), \tag{6}$$

φ is the work function for the specific conductor, $y = e(eE)^{1/2}/\varphi$, and the functions $t(y)$ and $\vartheta(y)$ are slowly varying dependences which can well be approximated by the expressions $t \approx 1$ and $\vartheta \approx 1 - y^2$.

Expression (5) holds true under conditions that the emitter temperature is much less than the characteristic Fermi energy for the conductor and the exponential power is much higher than unity. This expression, called the *Fowler – Nordheim formula*, is convenient for treatment of experiments on EFE. The results of such experiments are usually represented as a dependence of $\ln(J/E^2)$ vs. $1/E$ or, which is the same, $\ln(J/V^2)$ vs. $1/V$ (V is the applied voltage). The rectilinear shape of this dependence implies that the electron emission mechanism is related to the field emission. Measuring the parameters of the dependence (the slope angle and points of crossing with the axes) allows, in principle, the determination of the area of the emitting surface and the magnitude of the electron work function, if the electric field strength E is known. In accordance with the Fowler – Nordheim formula, the EFE current density is very sensitive to the magnitude of the electron work function for the specific surface of the conductor. A notable current density (at the level of mA cm^{-2}) is reached at an electric field strength of the order of 10^7 V cm^{-1}. Expression (5) is modified easily taking into account temperature effects and also the real energy distribution of conduction electrons, which can be differed from the Fermi distribution (see, e.g., Refs [126, 128]).

In a real situation the current – voltage characteristics of EFE may be different from the simple model expression (5). This is caused mainly by the presence of micro-nonuniformities, valleys and ridges on the surface of any emitter [126, 127, 129]. The electric field strength in the vicinity of such a ridge may exceed the relevant average value, determined as the ratio of the voltage V applied to the gap to its length L, by many times. This phenomenon is called the effect of the field amplification on nonuniformities. Due to this effect the EFE current in usual real conditions exceeds that determined on the basis of the Fowler – Nordheim expression (5) by 1 – 2 orders of magnitude. The factor

$\beta = E/V$ has been used as a quantitative measure of the effect of amplification of the electric field in the vicinity of a conductor surface. Here, E is the electric field strength near the conductor surface, and V is the applied voltage. In the event of a perfect smooth surface $\beta = 1/L$. In the case of a cylindrical ridge ended with a spherical cap of radius R, the magnitude of the parameter sought $\beta \sim A/R$, where A is the numerical factor close to 0.2 [129]. Thus, the electric field strength in the vicinity of a sharp ridge, which is characterized by the aspect ratio $L/R \gg 1$, is about $0.2L/R$ as high as the volumetrically averaged magnitude.

The amplification factor of the electric field is very sensitive to the geometry of the ridge. Due to an uncertainty in the size and shape of ridges on real surfaces, the quantitative evaluation of this factor is possible only within a numerical coefficient. Besides, micro-nonuniformities existing on the surface of any conductor are characterized by some spread in size and geometry. Thus, each of these nonuniformities is acted on by the electric field strength of various magnitudes, which causes a spread in the relevant current–voltage characteristics. Nevertheless, the character of dependence of the EFE current on the applied voltage for a real conductor is described quite well by the Fowler–Nordheim relation (5). This is described largely by the smoothing action of the logarithmic dependence which is used routinely for the analysis of experimental data.

A standard procedure for processing the experimental dependence of the electron field emission current density on the applied voltage on the basis of the Fowler–Nordheim relation (5) suggests the work function of the emitter material φ to be known. This allows, in principle, the evaluation of the amplification factor of the electrical field strength and the area of the emitting surface $A = I/j$. If the magnitude of φ is unknown, as is the case for CNT-based emitters, it can be determined on the basis of measurements of the energy distribution of emitted electrons. Namely, as follows from expressions (4), (5), the energy distribution function of electrons emitted by a metal surface subjected to the action of an electric field E at moderate temperatures has the following form [128]:

$$\frac{\mathrm{d}j}{\mathrm{d}\varepsilon} = \frac{me^2E}{h^2 t(y_0)\sqrt{2m\varphi}} \exp\left(-\frac{C_2}{E}\right) \frac{\exp(\varepsilon/d)}{1+\exp(\varepsilon/T)}. \qquad (7)$$

As is seen, the parameter

$$d = \frac{ehE}{4\pi\, t(y_0)\sqrt{2m\varphi}} \qquad (8)$$

depends on the ratio $f = \varphi^{1/2}/\beta$. This allows fitting the measured distribution to expression (7), using f as a fitting parameter. The magnitude of f, determined in such a manner, is inserted into the Fowler–Nordheim expression, whence the values of the electron work function φ and amplification factor β of the electric field strength are determined. Besides, the emitting surface area can be determined by the point of crossing of the Fowler–Nordheim dependence (5) with the ordinate axis.

The energy distribution of emitted electrons is determined by two factors: the low-energy wing is determined by the tunneling probability, while the high-energy wing is determined by the character of the energy distribution of electrons in a metal, i.e. by the emitter temperature. The width of the emitted electron energy distribution is about linear with the electric field strength, while the peak of the spectrum remains close to the Fermi level.

Electron field emission of carbon nanotubes. Good emission properties of CNTs are caused mainly by the high aspect ratio inherent to these objects. As a consequence, the electrical field strength in the vicinity of a nanotube is hundreds times higher than the volumetrically averaged value estimated as the ratio of the applied voltage to the gap length. Therefore, the emission properties of CNTs manifest themselves at considerably lower magnitudes of applied voltage in comparison with standard electron field emission cathodes which are fabricated on the basis of macroscopic sharpened metallic tips and are used conventionally. This offers the possibility for designing CNT-based displays and cathode luminescent light sources, which are distinguished by a considerably lower operating voltage and energy consumption in comparison with existing devices of similar appointment.

The peculiarities of the carbon nanotube EFE can be understood using the above-presented views about the mechanism of EFE of conductors, including the role of the surface geometry and effect of the electric field strength amplification. However, one should take into account that the character of the EFE of nanotubes differs from the above-described ideal picture in many respects. These differences concern firstly the anisotropy in electronic characteristics of a CNT. Correspondingly, the electron energy distribution also possesses a high anisotropy and differs considerably from the Fermi distribution (4). As follows from the analysis presented above, the nanotubes constituting a real sample can possess various electronic characteristics. Depending on such structural features as chirality and diameter, they can behave either like a metal or semiconductor with the energy gap width inversely proportional to the diameter. This causes a considerable spread in the emission properties of individual nanotubes constituting a macroscopic sample. Thus, the emission characteristics of such a sample are a result of averaging over a large number of individual nanotubes and may differ notably from the above-described ideal model represented by the Fowler–Nordheim relationship (5). Nevertheless, for the most part the current–voltage characteristics of EFE for macroscopic nanotube samples corresponds qualitatively to this expression, which is convenient in processing and analyzing experimental data. However, the magnitudes of relevant fitting parameters may differ considerably from the real values of the work function and electric field strength amplification factor characterizing the specific sample.

High emission properties of CNTs were first demonstrated by the authors of works [24, 25]. In paper [24], multiwalled nanotubes aligned perpendicularly to the substrate plane were used as an emitter. The area of the emitting surface was evaluated as 1 mm^2. The emission current–voltage characteristics measured in high vacuum conditions are in good agreement with the Fowler–Nordheim function (5) providing that the electric field strength amplification factor is about 1000 and the work function is equal to 5 eV. As measurements demonstrated, the emission current density of about 50 mA cm^{-2} is reached at the voltage across the gap of about 500 V. In works [25], both the single-walled and multiwalled nanotubes were studied as a source of the electron field emission. The emission current–voltage characteristics of CNT films, measured at room and some higher temperatures are in good agreement with the Fowler–

Nordheim dependence inherent to the electron field emission. A rise in the temperature causes some contribution of the thermal electron emission. The latter comes to prevail at 745 K. The maximum emission current density was as high as 3 A cm^{-2}.

The electron field emission of single-walled nanotubes was first observed in work [130]. The nanotubes were produced in an arc discharge with a Fe/Ni catalyst. The material containing nanotubes was taken from the camera walls. This material was flooded with distilled water and ultrasonicated for 12 h at $T = 373$ K. Then fullerenes were extracted from that sample by means of toluene, which was followed by holding under air for 20 min at $T = 543$ K in order to remove amorphous carbon. Then the material was treated with hydrochloric acid, which promoted the removal of metal particles. The above-described procedures resulted in a black thin layer of a paper-like material of about 0.1 mm in thickness. A thin rod less than 0.1 mm in thickness and of 1 – 2 mm in length was cut out from this material. This rod was attached by means of a graphite-based cement to a tip of tungsten or Ni/Cr alloy wire of 0.3 mm in diameter.

SEM observations indicated a plethora of microbundles of 30 – 40 nm in diameter, sticking out of the rod. Each of the bundles contains about 400 – 800 single-walled nanotubes of about 1.3 nm in diameter. These nanotubes are practically inseparable from the bundle even using ultrasonication in toluene. The emitter tip was spaced at 30 – 50 μm from a luminescent screen of 100 mm in diameter. The emission was studied at room temperature and a pressure of 3×10^{-8} Torr. At the emitter voltage of 420 V, one could observe the emission from one of the bundles, which was sticking out of other microbundles. A further rise in voltage up to 520 V caused the emission of many (about 10) microbundles, which brought into existence several glowing spots on the screen. At a voltage of 1000 V and an interelectrode gap of 30 μm, the field emission current reached 32 nA and remained stable within an accuracy of 7% for 10 min. In a period of 10 days a smooth two-fold irreversible decrease in the emission current was observed. The current – voltage emission characteristics were in agreement with the Fowler – Nordheim dependence. Processing this dependence under the assumption that the work function of a single-walled nanotube is equal to that of graphite (4.6 eV) and the electric field strength amplification factor on a surface of a conductor is expressed by the relation $\beta = E/V = 1/(5R)$ results in the value of $R = 30$ nm. This magnitude considerably exceeds the radius of an individual nanotube, but is comparable with that of a microbundle. Thus, one can conclude that the emission occurs not from individual nanotubes, but from microbundles as a whole.

One should mention difficulties emerging in processing the emission current – voltage characteristics of nanotubes on the basis of the Fowler – Nordheim relation (5) in order to determine the electric field strength amplification factor, work function and the area of the emitting surface. These parameters determining emission properties of nanotubes are involved in relation (5) in some combination, and they cannot be extracted in the pure state from the current – voltage characteristic observed. As a source of supplementary information, which allows the resolution of the above-stated problem, the measured energy distribution function of emitted electrons can be employed.

The above-described procedure was followed by Fransen et al. [128], who studied emission properties of individual multiwalled nanotubes of 44 and 9 nm in diameter, having closed ends and attached to a tungsten tip by means of a graphite-based conductive cement. Contamination was removed through high-vacuum conditioning for 30 s at a temperature of about 1000 K. Increasing the applied voltage from 460 to 1100 V provided a linear decrease in the position of the peak in the energy distribution of emitted electrons by a factor of -1.6 mV V^{-1}. The magnitude of the parameter $f = \varphi^{1/2}/\beta = 3.54 \times 10^{-7}$ $eV^{1/2}$ m was determined through the statistical processing of a large set of energy dependences of the number of emitted electrons, measured at various values of the applied voltage. A typical emission current – voltage characteristic of one of the samples is given in Fig.15 in the Fowler – Nordheim variables. The processing of this characteristic taking into account the above-given magnitude of f allowed the determination of the electric field strength amplification factor $\beta = (7.6 \pm 0.5) \times 10^{-6}$ m^{-1}, the electron work function $\varphi = 7.3 \pm 0.7$ eV and the emitting surface area 9.8×10^{-16} m^2. One should note that the latter value is about half the cross section of the nanotube under investigation, whose diameter is 44 nm. It is apparently caused by the absence of several layers in the nanotube structure.

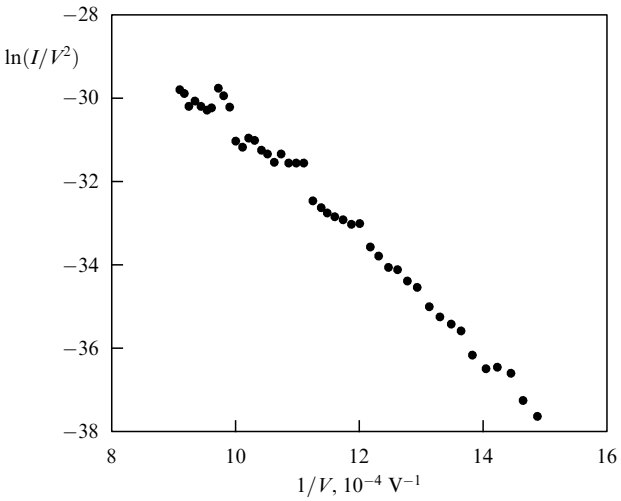

Figure 15. Emission current – voltage characteristic of an individual multiwalled nanotube, plotted in the Fowler – Nordheim coordinates [128].

The Fowler – Nordheim model considering the electron field emission as under-barrier tunnelling of the conduction electrons under the action of an external electric field is generally applicable to metallic emitters. Since a nanotube is typically a semiconductor, the theory has to be modified in a proper manner, taking into account the possible electron and hole conduction, real magnitude of the electron effective mass, real arrangement of valence and conduction bands and also the possibility of penetration of the electric field inside the material. A consistent approach to the solution of this problem has been presented, in particular, in works [131 – 132], where a semiconductor is modelled by a metal surface covered with a semiconducting film. In doing so, the penetration of the electric field inside a semiconductor is allowed. A linear decrease of the potential therewith takes place in relation to a metal – semiconductor interface, and the electron emission occurs from either the top of the valence band or the bottom of the conduction band. However, the electron field emission current – voltage characteristics are described in both cases by the Fowler – Nordheim expression

involving the magnitude of the electron work function, modified in a proper way. In this case a maximum in the energy distribution of emitted electrons is displaced linearly toward lower energies with a rise in the electric field strength.

The application of the above-considered theoretical approach to the description of emission properties of CNT-based emitters is hindered by the considerable spread in structural parameters of nanotubes constituting the emitters. Thus, a material produced with present-day synthesis processes contains a set of single-walled nanotubes of different chiralities and, therefore, of various electron structures [38, 133–134]. As to multiwalled nanotubes, each of them apparently consists of some number of single-walled nanotubes of diverse chiralities. Therefore, a multiwalled nanotube contains elements possessing various electronic and, consequently, emission properties. A consistent theoretical description of a material consisting of a large number of such tubes with dissimilar characteristics is hardly possible now. Besides, the situation is complicated by the fact that some nanotubes involved in real emitters have open ends, while the others possess closed ends. Existing theories which consider the electron field emission of CNT-based materials (see, for example, paper [128]) do not discriminate these structures and only give a qualitative description of the process mechanisms.

It is believed traditionally that the source of the electron field emission from CNT is its end cap, in the vicinity of which the electric field strength is a maximum. However, recent studies [135–138] demonstrated that a lateral surface of nanotubes also serves as a quite good source of the electron emission. The density of current emitted from a lateral surface is generally much less than that for the end cap. However, at some orientations of a nanotube relative to the direction of the electric field the contribution of the lateral surface emission to the total current can turn out to be prevailing, since the area of the lateral surface exceeds naturally that of the end cap.

Dependences of the electron emission current of multiwalled nanotubes on their orientation relative to the electric field vector were studied in detail in work [135]. Poly-crystal nickel plates of $10\times5\times0.3$ mm in size were used as a catalyst and, simultaneously, as a substrate. The surface of the plate was subjected for 10 min to the action of an electrical discharge with a current density of 50 mA cm^{-2}. This provided the surface with a porous structure promoting the nanotube growth. The nanotubes were grown by the plasma chemical deposition method, as a result of electrical discharge in an N_2 and CH_4 mixture at a current density of 15 mA cm^{-2}. If the anode was situated directly above the substrate surface (orientation $O_\perp$), the nanotubes were aligned perpendicular to the surface. In the case when the anode was oriented at an angle of 45° to the substrate surface, the nanotubes were aligned at an angle of 45° to the surface (orientation O_{45}). A layer of nanotubes aligned in parallel to the substrate surface (orientation $O_\square$) was obtained through sleeking the nanotubes aligned at an angle of 45° with a smooth teflon rod.

SEM and STM investigations indicated that the multiwalled nanotubes obtained are distributed homogeneously over the substrate surface and have a surface density ranging from 10^8 to 10^9 cm^{-2}. Their diameter, depending on the discharge current and the temperature of the substrate, ranged from 100 to 200 nm. Emission properties of these nanotubes were investigated at room temperature in a vacuum of 5×10^{-7} Torr. A copper wire loop of 3 mm in diameter was used as an anode. It was spaced at 80 μm from the emitter and was fixed by means of a mica film. The emitting area was 1 mm^2.

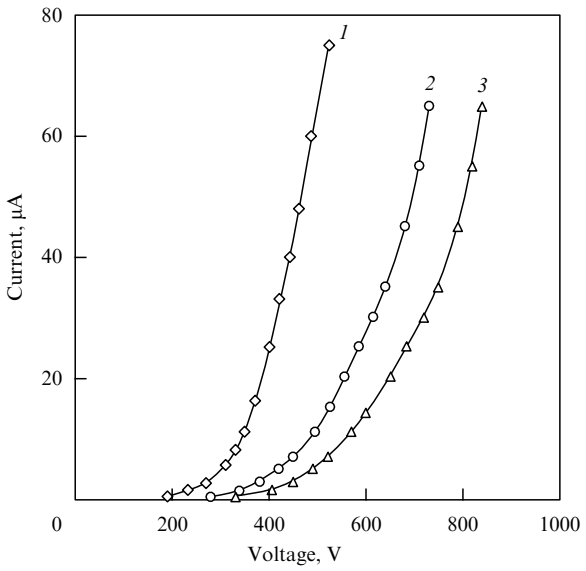

Figure 16. Field emission current–voltage characteristics of multiwalled nanotubes arranged in various ways relative to the substrate plane [135]: *1* — alignment in parallel to the substrate plane; *2* — alignment at an angle of 45° to the substrate plane; *3* — alignment normal to the substrate plane.

The emission current–voltage characteristics measured at various orientations of nanotubes relative to the substrate surface are given in Fig. 16. The threshold magnitude of the electric field strength, determined by the minimum detectable emission current of 0.5 μA, is estimated as 2, 3.5 and 4 V μm^{-1} for orientations $O_\square$, O_{45} and $O_\perp$, correspondingly. As is seen, the emission current depends significantly on the orientation of the CNTs relative to the substrate surface. An emission current of 1 mA cm^{-2}, providing the operation of flat panels, is reached at the electric field strength of 4.2, 6 and 6.8 V cm^{-1} for the three orientations, respectively. The processing of the current–voltage characteristics using the Fowler–Nordheim variables: $\ln(I/V^2)\sim(1/V)$ results in a linear shape of the relevant dependences, which implies the prevalence of the electron field emission mechanism. The occurrence of the electron field emission from the longitudinally aligned CNTs can be attributed to the existence of defects in the nanotube structure. This explanation implies that the threshold electric field for the longitudinally aligned nanotubes is lower than that for the orientations O_{45} and $O_\perp$. Another reason for the rise in the threshold electric field strength as the nanotube alignment comes to the perpendicular orientation may be related to the presence of a metal particle inside the end cap of a nanotube, which can retard the emission and enhance the emission threshold field in the case of orientation $O_\perp$. Moreover, an inclined nanotube possesses a larger active surface and therefore can emit more electrons.

Emission properties depend not only on the geometry of an individual nanotube, but also on its surroundings. It is easy to realize that in the case of a close arrangement of similarly aligned nanotubes the electric field strength amplification factor should be significantly less than that in the case of an individual nanotube appearing as a sharp ridge over a flat substrate surface. This intuitive reasoning is supported by the results of numerical calculations of the electric field potential

(a), the electric field strength amplification factor (b) and the electron emission current density (c), obtained for various mean distances between emitters and presented in Fig. 17 [139]. The calculations were performed for nanotubes of 1 μm in height and 2 nm in diameter, which fill the substrate surface homogeneously, but with varied density. As is seen, there exists an optimum distance between nanotubes (about 2 μm), corresponding to the maximum electron emission current density. The existence of the optimum stems from the fact that at low emitter density the emission current density increases as the surface emitter density rises, while at a high emitter density this increase is retarded by the relevant lowering in the electric field strength amplification factor of an individual emitter. A more general conclusion leans upon the fact that the distance between emitters, which is optimum from the viewpoint of the emission current density, is about twice as large as the height of an individual emitter. This corresponds to an optimum magnitude of the emitter density of 2.5×10^7 cm^{-2} or 625 emitters per pixel of 50×50 μm in size. The limiting case of zero distance corresponds to a flat metallic surface.

The above-given conclusion about the dependence of emission properties of the two-dimensional assembly of nanotubes on their surface density was supported by experiment [139], where an original way for depositing an iron catalyst onto a silica substrate was employed. In doing so, a catalytic dye containing 10 – 60 mM solution of $Fe(NO_3)_3 \cdot 9H_2O$ in ethanol was deposited via stamping onto a substrate. The patterns obtained were placed into a reactor, where nanotubes were grown as a result of thermal catalytic decomposition of acetylene in the presence of N_2 at a temperature of 720 °C. This resulted in the formation of a matrix consisting of films of multiwalled nanotubes of about 15 nm in diameter and 5 μm in height. Each line in the matrix was 10 μm in width and the separation between lines was 50 μm. The rise in the solution concentration was accompanied by an increase in the surface density of nanotubes in the film.

Electron field emission of the samples was studied in a vacuum setup (rest pressure of about 10^{-7} mbar) equipped with a luminescent screen and an image-scanning device. The emission current was measured at a constant voltage between the cathode and the screen (3000 V) and varied interelectrode gap. The scanned surface amounted 200×200 μm in area and was divided into 100×100 pixels. A platinum – iridium rod having a cap of 2 – 5 μm in radius was utilized as an

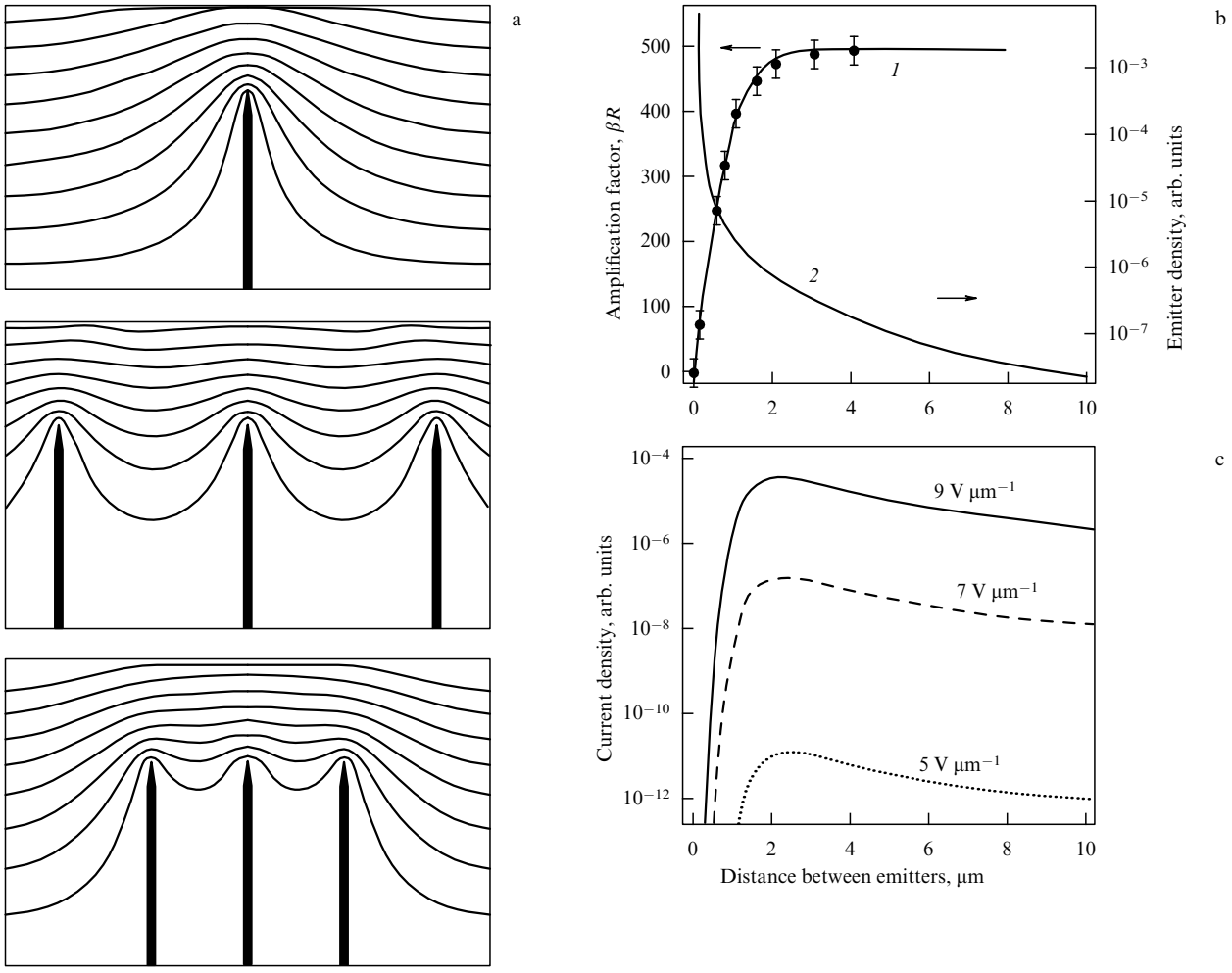

Figure 17. Spatial distribution of the electric field and the emission characteristics of single-walled vertically arranged nanotubes 1 μm in length and 4 nm in diameter, as calculated at various magnitudes of the mean separation between them [139]: (a) equipotential lines of the electrostatic field for distances between tubes of 4 (upper picture), 1 (middle picture) and 0.5 μm (lower picture); (b) dependence of the electric field strength amplification factor (*1*) and the emitter density (*2*) on the average distance between tubes; (c) dependence of the emission current density on the average distance between emitters for various mean electric field strengths.

anode, which was subjected to a voltage of 100 V. The separation between the anode and the surface of the emitting film ranged from 3 to 5 μm. The field emission current was measured depending on the anode tip position. In so doing the noise level did not exceed 1 nA. The measurements showed a rather weak dependence of the total field emission current on the surface density of nanotubes. In all cases the emission starts at a relatively low field (2–3 V μm^{-1}) and exhibits a high degree of nonhomogeneity. The emission originates from a relatively small number (< 100) of dots, spread in an arbitrary manner over all the cathode surface. This implies that the emitters having a low length/diameter ratio do not make any contribution to the emission, because they have a relatively low electric field strength amplification factor. Therefore, the number of emitting dots should depend on the area of the surface under investigation. A surface of about 1 cm^2 in area emits only from ridges having enhanced electric field strength amplification factor ($\sim$ 1000), while a site of about 100 × 100 μm in area may not contain such dots, so that dots with a lower amplification factor $\sim$ 100–200 provide the emission. Whence follows that the emission current–voltage characteristics obtained with micrometer resolution should depend on the surface density of nanotubes. The existence of such a dependence is revealed by the measurements of the surface distribution of the emission current density, performed at a various densities of nanotubes. In the cases of high and low density there are a few emission sources which are spread over the surface in an arbitrary manner. The best result is reached at a moderate density of nanotubes, when the surface structure of the source is easily resolved. Poor emission from films with a high surface density of nanotubes is caused by the electrostatic screening effect of neighboring emitters. For this reason, the electric field strength in the vicinity of a nanotube cap in the case of closely spaced nanotubes is lower than that in the case of widely spaced ones.

In accordance with the Fowler–Nordheim expression (5), the field emission current density is a monotonically increasing function of the applied voltage. In reality this rise is observed only within a limited range of applied voltages. In exceeding some magnitude of the voltage the rise in the current density is practically terminated, reaching a saturation value. The current saturation effect in CNT-based field emitters is their advantage, because in conventional emitters one should use additional transistors connected in series for restricting the current. The maximum values of the CNT electron emission current measured by various authors are characterized by a spread over several orders of magnitude. This implies the existence of several, but not one, mechanisms of limitation of the CNT electron emission current, which manifest themselves depending on the conditions of production and purification of the material.

The above-mentioned mechanisms of current limitation were studied in detail in works [140–142]. As the object of investigation either a film consisted of several single-walled nanotubes of about 1.7 μm in length, purified via thermal methods and pressed into an elongated filament-like structure or an individual nanotube was used. Nanotubes of 90% in purity were produced in the form of a colloidal suspension containing 0.3 mg of nanotubes per millimeter and 0.5 wt.% surfactant. In order to separate individual nanotubes from bundles the suspension was filtered, which was followed by addition of 0.1 mg ml^{-1} solution of N, N-dimethylformamide and subsequent processing in an ultrasonic bath for 24 h. The nanotubes obtained were attached to a tungsten filament loop, which was used as a thermal ion source of electrons in scanning electron microscopes. The electron field emission was studied at a constant voltage in a vacuum of 10^{-9} Torr. The interelectrode gap was equal to 2 cm. The current–voltage characteristic of an individual single-walled nanotube is presented in Fig. 18a. As is seen, at low voltages it is in good agreement with the Fowler–Nordheim theory. However, a further rise in voltage (above 1000 V) results in the saturation of the measured current which deviates more and more from the corresponding Fowler–Nordheim magnitude. At high voltages (1600–1800 V), the deviation is 100–10,000 times. The saturation effect is accompanied by a 20-fold increase in the emission current fluctuation frequency and a notable change in the visual appearance (under microscope) of the emission source.

The detailed studies performed by the authors of work [140] demonstrated that the main mechanism of restriction of the emission current relates to the existence of adsorbed impurity atoms on the emitting surface. This causes an

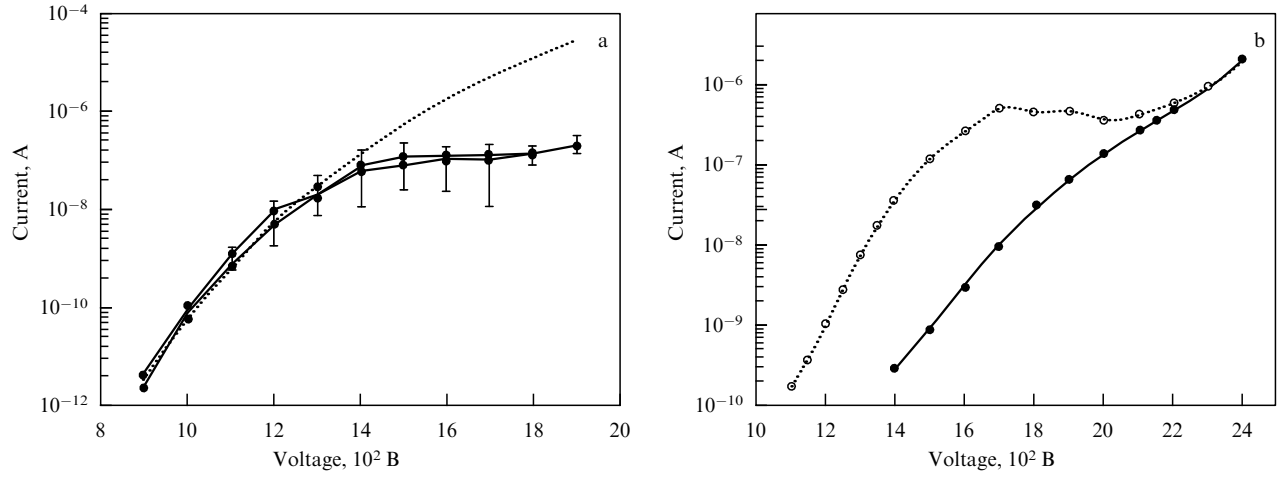

Figure 18. (a) Current–voltage characteristics of an individual single-walled nanotube. The dotted line shows the calculated Fowler–Nordheim dependence (5); (b) current–voltage characteristics of an individual single-walled nanotube in the presence (dotted line) and absence (solid line) of adsorbates [140].

increase in the emission current of about two orders of magnitude. A careful purification of the CNT surface from admixtures, performed through the vacuum heating of a sample up to 900 K, results in a lowering of the emission current by two orders of magnitude, suppressing the fluctuations in the emission current and eliminating the current saturation effect. In this case the current – voltage characteristic is in good agreement with the Fowler – Nordheim dependence up to a current magnitude of about 2 μA (Fig. 18b). The author's conclusion about the important role of adsorbates has been supported by the experiment, where H_2O adsorbates were inserted artificially, holding the emitter under the partial pressure of water vapor of 10^{-7} Torr for 5 min. This resulted in a 200 times increase in the emission current at a voltage of 1400 V and the current saturation at a level of 100 – 300 nA. Therefore, one can conclude that the emission characteristics of CNTs are very sensitive to the degree of purification of the material, as well as to the quality of the vacuum system. This conclusion lowers the optimism of developers of CNT-based electron emitters.

Even more complicated behavior of the emission current – voltage characteristics of individual single-walled nanotubes has been found in work [141] by the same authors, who performed measurements at a pressure of 10^{-9} Torr and various temperatures. The soot was produced in an electric arc discharge using Fe and Ni catalysts. It contained about 5 vol.% of isolated single-walled nanotubes 0.7 – 1.2 nm in diameter as well as similar nanotubes bound into bundles. The soot was attached to a thermal ion filament placed on a standard ceramic base. The filament served for heating the nanotubes up to the desired temperature. The emission current was measured at a distance of 5 cm between the emitter and the phosphor film, the applied voltage varied between 1700 and 2600 V and the temperature ranged from 300 to 1800 K. At a low temperature (below 700 K), the emission mechanism relates to the presence of adsorbed particles on the surface of nanotubes. Heating above 900 K promotes the removal of these particles from the surface, which is accompanied by a lowering in the emission current by two orders of magnitude (from 2 μA down to 0.02 μA). Subsequent cooling of the sample down to 300 K brings about the recovery of the initial current for several tens of seconds. This is caused by the presence in the vacuum chamber of a trace quantity of H_2O, CO and CO_2 (on the level of 10^{-9} – 10^{-10} Torr) originating mainly from the luminescence screen. If the screen is subjected to thermal processing for 2 h in vacuum at 50 – 60 °C, the initial emission properties of the emitter can be restored already in about 60 min. In order to establish the origin of adsorbed particles affecting the emission properties of the emitter, the time dependences of the emission current have been measured on filling the vacuum system with small quantities of various gases and vapors. The experiments have shown that the recovery of the emission current upon cooling takes 70 min on filling with water vapor at a pressure of 5×10^{-9} Torr, 37 min at 5×10^{-8} Torr H_2O, 16 min at 4×10^{-7} Torr H_2O, and 9 min at 5×10^{-6} Torr H_2O. Inserting H_2, CO and CO_2 in the same quantity does not affect the time of recovery of the emission current. As follows from the measurements, the emission current of single-walled nanotubes with adsorbed gases exhibits a high level of low-frequency noise (fluctuations) which rises exponentially with temperature. Thus, the level of fluctuations at 700 K is 20 times higher than that at room temperature. However, at a temperature above 900 K adsorbates are eliminated, and the noise level decreases below the corresponding magnitude at 300 K. Hence it has been revealed that the fluctuations of the emission current are caused by adsorbates.

The current – voltage characteristics of pure single-walled nanotubes at $T = 1000$ K are in good agreement with the Fowler – Nordheim dependence. However, the temperature dependences of the emission current of pure emitters, measured at varied applied voltages, failed to fit with the Fowler – Nordheim formula. The experimental dependence has a linear shape, while the standard theory provides a quadratic in temperature dependence. Further heating of a sample above the temperature of 800 – 1800 K, whose exact magnitude is linear with the applied voltage (with the proportionality factor of 1.2 K V^{-1}), is followed by the transition of the emitter into a new state distinguished by even lesser emission current. Nevertheless, even in this case the current – voltage characteristics are well described by the Fowler – Nordheim formula, while the electron work function which fits this dependence is about twice as high as that at low temperatures.

The existence of two emission states of single-walled nanotubes distinguished by the presence or absence of surface adsorbates was confirmed in recently published work [143]. The samples used were single-walled nanotubes of 90% purity, 1.2 nm in diameter and 0.2 – 2 μm in length, bound into bundles. The samples were produced by the laser ablation method and catalyst particles Ni/Co were observed as a major contaminant. The material was dispersed in toluene of 1.4 mg ml^{-1} in concentration, whereupon the suspension obtained was applied as a thin layer over a flat Co substrate 1 cm^2 in area. The flat metallic cathode contained a small hole of 500 μm in diameter providing the passage of emitted electrons. This allowed measurement of the electron energy distribution function by means of an electron spectrometer. The spacing between the anode and cathode was 0.61 mm. Before inserting the sample into the vacuum chamber for measuring the emission current, it was held in high vacuum for 7 hours at 400 °C. The emission current was measured in vacuum conditions of 10^{-10} Torr. Unlike the above-cited work [141] where adsorbates were removed from the nanotube surface through heating the sample up to 900 K, in the considered work [143] they were removed by means of high applied voltage ($\sim$ 1000 V). The shape of the emission current – voltage characteristic depended significantly on the conditions of pumping out, which is an indirect indication of the role of adsorbates. Thus in conditions of poor vacuum the current – voltage characteristics had a reversible character, i.e. they did not depend on the direction of alternation of the voltage. The energy spectra of emitted electrons show a linear dependence of the spectral maximum on the applied voltage. This dependence is characterized by a higher slope in comparison with the case of pure nanotubes, however these two straight lines cross each other at a voltage of 1000 V. At this point adsorbates are fully removed. The measured electron energy spectra point up the possible position of the resonance level caused by adsorbates, which resides 0.9 eV below the Fermi level. The existence of this level enhances the electron tunnelling probability and explains the increased magnitude of the emission current.

Electron work function of CNTs. The emission properties of a nanotube are determined largely by its electron work function. Experimental data about the magnitude of this parameter, now obtained by various authors, differ from

each other very much. This is caused by distinctions in the electron structure of nanotubes produced in different conditions, which is reflected in the electron work function. Some tubes are ended with unclosed caps, which also undeniably changes the magnitude of this parameter. Besides, the nanotube surface may contain such radicals as CO, OH, NO, etc. either as sorbents or adducts which introduce additional states into the electron spectrum of a nanotube and can change the electron work function. In this connection the use of a common magnitude of the electron work function for the description of a material containing nanotubes seems rather a matter of convention and may be considered as a result of averaging over some, quite wide distribution of values.

Two approaches were elaborated for determining the electron work function of CNT, which often result in rather different data. The first of those (I), described partly above, is based on processing the measured emission current – voltage characteristics of nanotubes using the Fowler – Nordheim expression (5). The application of this approach requires either detailed information about the nanotube structure or additional data about the emitted electron energy distribution. The second approach to evaluating the electron work function of CNTs (II) is based on the determination of the energy spectrum of photoelectrons emitted on optical irradiation of the material surface. The lower boundary of the spectrum corresponds to the electron work function.

Table 3 presents the magnitudes of the electron work function of CNTs, measured and estimated by various authors. As is seen, in most cases the magnitude of the CNT electron work function is close to that for graphite, which ranges between 4.4 and 5 eV. A notable distinction between the magnitudes of the work function for single-walled and multiwalled nanotubes was not observed. The estimate of the work function (0.2 – 2 eV) submitted by A N Obraztsov with collaborators [149 – 154] is markedly apart from the total mass of data. However, this estimate is rather indirect, and its result depends substantially on the curvature radius of the emitter used in the calculation, which is determined in this context on the basis of visual analysis of microphotographs. One can suppose that in this case the electron emission originates from an open end of a nanotube, so that the characteristic size of the emitting surface is several times smaller than the diameter of the nanotube, which is used in estimation of the electron work function. The statistical treatment of the electron work function data given in Table 3 without taking into account the last row in this table results in the averaged value of $\varphi = 5.26 \pm 0.85$ eV.

As follows from the analysis of works addressed to determine the electron work function of CNTs, many questions related to this problem remain unsolved. It is unclear how this magnitude depends on both the diameter and chirality of a single-walled nanotube. It is not established what determines the electron work function of a multiwalled nanotube consisting of single-walled nanotubes with definite magnitudes of the work function. There are no data in hand about the dependence of the electron work function on the position of the emitting area on the nanotube surface, as well as on structure defects and bendings of the surface of single-walled and multiwalled nanotubes. One can hope that further studies focused on answering those and other similar questions, coupled with the development of methods for synthesis of nanotubes with pregiven structural parameters, should provide a possibility for production of CNT-based electron emitters having well-defined emission characteristics.

Table 3. CNT electron work function measured and estimated by various authors.

A type of nanotube	Diameter, nm	Measurement method	Work function, eV	Reference
Multiwalled	44	I	7.3 ± 0.7	[128]
Single-walled	1.0 – 1.4	II	4.65 ± 0.1	[144]
Single-walled	1.4	II	4.8	[145]
Multiwalled		II	5.7	[146]
Multiwalled		II	4.3	[147]
Multiwalled	10	II	4.95	[148]
Single-walled	1.4	I	5.1	[138]
Multiwalled	10 – 50	I	0.2 – 2	[149 – 154]

6. CNT-based cold cathodes

Flat displays. The above-described results of investigations into emission characteristics of CNTs form the basis for the development of electron devices with CNT-based cold cathodes. This class of devices involves electron displays, X-ray sources, luminescent light sources, etc. and is distinguished from conventional analogues by a reduced applied voltage and power supply, low weight and small transverse size. A short review of works addressed to the development and optimization of electron devices with CNT-based cold cathodes is presented below.

A cold cathode used in an electron device as a source of electron emission must meet the following main requirements:

(1) high stability of the current;

(2) high brightness of the source;

(3) low spread in the energy of emitted electrons;

(4) high surface homogeneity of emission characteristics of the emitter.

As follows from the above-described investigation data, CNT-based cathodes meet the just formulated requirements quite well and are highly competitive in respect to the listed parameters with the most widely used commercial field emission sources. Thus, the already cited work [128] reports the measured stability of the emission current of multiwalled nanotubes over 54 days. The measurements were performed at a vacuum below 2×10^{-12} Torr. The current was recorded every 10 s. In accordance with the experimental findings, the current ranged smoothly between 400 and 435 nA during the period of 54 days, showing a short-time stability at the level of 1.2%. Long-time variations in the emission current are attributed by the authors to oscillations in the voltage of the power supply. The brightness of a CNT-based emitter easily reaches that of conventional emitters. As for the energy spread of emitted electrons, its magnitude depends on the electronic properties of the emitter. The magnitude of the energy spread is narrower in the case of a semiconducting emitter than for a metallic one and is determined by the width of the spectral peak in the local density of states in the vicinity of the nanotube cap.

High surface homogeneity of emission characteristics is reached as a result of employing a special-purpose technology for nanotube growth. The result of these efforts is determined mainly by the properties of the substrate surface. Thus, recently published work [155] reported on the development of a field emitter with a substrate in the form of a thin film of

anodized aluminium oxide (AAO) deposited onto a silicon plate. Two types of samples have been used as the raw material. In the first case (AL), the Al film 12 μm thick was deposited directly onto a silicon plate, and in the second one (ALNB) an Al film 400 nm in thickness was deposited onto a silicon plate coated with a layer of Nb. The surface of the AL sample was subjected to electropolishing up to a mirror shining state in a mixture of hydrochloric acid and ethanol solution. The ALNB sample contained 2 at.% Nb, which provided a smooth surface. This allowed one to conduct the electrochemical anodization of its surface without electropolishing. In both the cases the anodization was performed at 15 °C by means of a 0.3 M solution of oxalic acid. The anodization voltage was kept at 40 V. The ALNB sample was anodized at a current density of about 7 mA cm^{-2}, which then sharply decreased to 0.2 mA cm^{-2}. This was followed by a change in the surface color, which served as indication of the completion of the anodization procedure. The full anodization of an Al layer took 2 – 3 min. The corresponding anodization of ALNB took 10 min. The diameter of pores formed as a result of anodization was on average 12 – 13 nm. The depth of pores amounted to 0.5 and 1 μm in the case of samples ALNB and AL, respectively. In order to lower the thickness of the barrier layer the AAO pattern was held for 30 min in 0.1 M phosphorous acid at 30 °C. This gave rise to an increase in the diameter of pores to 70 – 80 nm. A cobalt catalyst was placed on the bottom of these pores using the electrochemical deposition method. The deposition was performed at a constant voltage from 5% $CoSO_4 \cdot 7H_2O$ solution stabilized by 2% H_3BO_3 solution. The voltage magnitude amounted to 15 V in the case of the AL sample. After a lapse of 1 min the aspect ratio of Co particles filling the pores amounted to 1. In the case of the ALNB sample, the Co deposition was conducted at a voltage of 3 V, so that no more than 10 s was required for obtaining the aspect ratio of 1. Reduction of the Co particles was performed for an hour under a flow of H_2 (2%) and Ar (98%) at 600 °C.

The nanotubes were grown during 15 min as a result of catalytic pyrolysis of C_2H_2 (10%), which was inserted into an H_2 (20%) and Ar mixture flowing at the rate of 200 cm^3 min^{-1} at a temperature of 650 °C. The field emission microscope and SEM observations demonstrated that multiwalled nanotubes grown on the ALNB substrate are 70 – 80 nm in diameter and of length ranging between 500 nm and several micrometers. As is seen, the nanotube diameter fits the characteristic size of pores. The nanotubes show a trend to orientation normal to the substrate surface. The nanotubes are very spread in length, and the longest of them are bent. It is noted that nanotubes do not grow from any of the pores filled with catalyst particles. Distinctions have not been found in the morphology of nanotubes grown on AL and ALNB substrates, with the exception of several broken nanotubes on the AL substrate.

The electron field emission from the emitter surfaces was studied using a glass plate coated with phosphor P22 and an In – Pb – O_2 layer as an anode. The emitter and the cathode were spaced at 260 μm. The emission current was measured at a vacuum of 2×10^{-7} Torr. The threshold electric field strength providing the emission current density of 10 μA cm^{-2} ranged between 1.9 and 2.1 V μm^{-1}. The emission current – voltage characteristics observed are in good agreement with the Fowler – Nordheim expression. Here the field amplification factor was estimated on the basis of these characteristics and under the assumption that the electron work function is equal to 5 eV as 520 and 3360 for the samples AL and ALNB, correspondingly. The main distinction between these samples relates to the surface density of multiwalled CNTs, which is higher in the case of the AL sample in comparison with that of the ALNB sample. This explains a lower magnitude of the field amplification factor in the first case. The extraordinarily high magnitude of the field amplification factor in the second case (3360) as compared with the standard estimate $\beta \sim 1000$ is caused by the lower surface density of nanotubes ($10^7 - 10^8$ cm^{-2}) in comparison with more typical values $10^9 - 10^{12}$ cm^{-2}.

Work [156], where a diode structure containing aligned nanotubes was firstly produced using the electrophoresis method, can be considered as an important stage in the development of electronic devices with CNT-based cathodes. Further progress in similar studies has culminated in the advent of the first fully sealed off displays involving a cathode with a CNT-based emitter. One of the first publications of such a kind is work [157], where a progenitor of a flat diode display of 1 cm in lateral size has been described. Multiwalled nanotubes bound into bundles were produced by the standard electric arc method; they were then dispersed in methanol and subjected to thermal treatment in air at 700 °C in order to remove contaminants. SEM observations

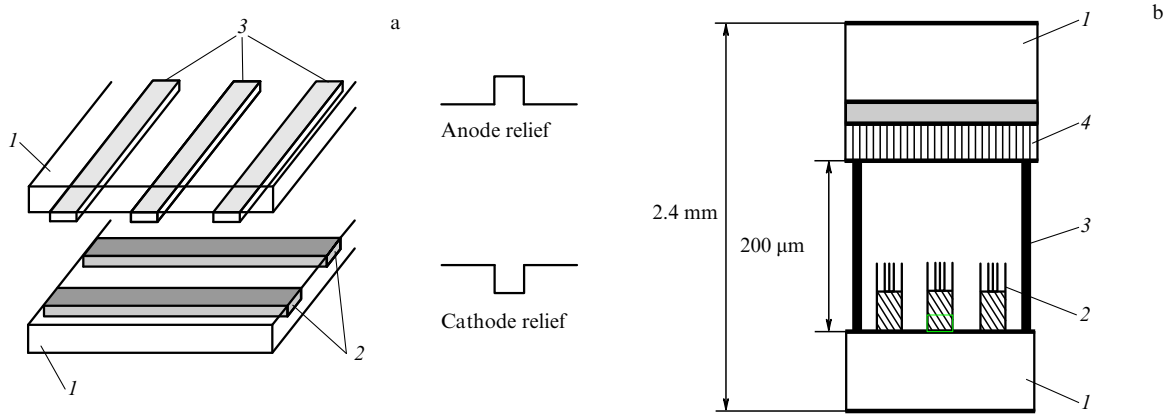

Figure 19. Construction scheme of fully sealed off displays with single-walled CNT-based cold cathode. (a) Prototype model [157]: *1* — glass substrates; *2* — stripes of epoxy resin containing nanotubes; *3* — phosphor stripes. (b) Color display of 132 × 113 × 2.4 mm in size [158]: *1* — glass plates of 1.1 mm in thickness; *2* — nanotube matrix with a metal substrate; *3* — separating plates; *4* — phosphor matrix.

showed that the thermal treatment resulted in an increase of CNT content in the samples up to 80%. Some nanotubes had open caps, while the others ended with conic caps of about 2 nm in the radius of curvature. The panel is sketched schematically in Fig. 19a. A glass substrate coated with parallel epoxy resin stripes containing 50 vol.% CNT was used as a cathode. Before coating the stripes of microchannels of 200 μm in width, 100 μm in depth and 300 μm in length were made on the cathode surface using hydrofluoric acid etching. The cathode surface density of nanotubes was about 2 μm^{-2}. As an anode a similar glass plate coated with phosphor stripes of 200 μm in width and 300 μm in length was employed. The spacing between the cathode and anode was kept at 30 μm. The CNT stripes were arranged perpendicular to those of phosphor, resulting in the formation of individual pixels at their intersections.

The emission current was measured at a pressure of 10^{-6} Torr. The current–voltage characteristics obtained for 16 various pixels spread over the emitter area of 1×1 cm were superimposed on each other with a high accuracy. This implies a high degree of surface homogeneity of the emitter. The instant emission current density of the pixels, required to drive a diode display (76 $\mu A\ mm^{-2}$), was reached at a voltage of 230 V. The measured current fluctuation level at a voltage of 300 V did not exceed 8% over 12 h. A legible image of a letter consisting of 12 pixels was displayed.

The design and practical testing of a 4.5-inch full-color display is the next stage in developing flat panel displays with CNT-based cathodes [158]. Figure 19b depicts schematically the display structure involving glass substrates 1.1 mm in thickness, one of which is coated with a patterned layer of single-walled nanotubes, and the second is coated with an $In/Pb/O_2$ phosphor layer. The separation between the substrates was kept at 200 μm.

Single-walled carbon nanotubes of about 1.4 nm in diameter and 0.5–2.0 μm in length were produced in an electric arc with graphite electrodes using the standard method, which was followed by purification with a 1:1 mixture of nitric and sulphuric acids at $T = 1000\,^{\circ}C$. The purified samples containing CNTs were cut into small pieces, washed with distilled water, dried and then ultrasonicated in isopropyl alcohol, which resulted in their dispersion. Thereafter the well-dispersed CNTs were mixed with an ultradispersed metal powder and an organic binder. The mixture obtained was applied over the substrate; then the binder was removed through thermal treatment at $T = 300\,^{\circ}C$ for 20 min. Metal particles were removed from the cathode surface using a surface rubbing process, causing the CNTs to protrude from the top surface. The anode surface was coated with phosphor layers involving Y_2O_2S : Eu, ZnS : Cu, Al and ZnS : Ag, Cl of 6–10 μm thick, corresponding to the red, green and blue colors, respectively. After thoroughly establishing the separation between the substrates the display panel was pumped out down to a pressure of 10^{-7} Torr and sealed off at $T = 415\,^{\circ}C$ in an ambient of highly purified Ar. The monitor manufacturing procedure is easily reproducible and scalable.

The monitor produced in such a manner of 4.5 inches in diagonal was used for formation of a color image with a high degree of surface homogeneity and time stability. It was tested using the green phosphor at an anode voltage of 800 V, which corresponded to an electric field strength of 4 V μm^{-1}, a duty of 1/4 and frequency of 15.7 kHz. A brightness of 1800 cd m^{-2} was achieved in the above-indicated conditions. Such high operating parameters of the display stem from the high degree of alignment of CNTs on the cathode surface, their considerable surface density and the good surface homogeneity of the cathode material.

One of the most attractive features of flat panel displays with CNT-based cathodes is the extraordinary low level of energy consumption, which relates to the low magnitude of the applied voltage. From this viewpoint a triode scheme appears to be more promising than the above-described diode scheme, so that the electron emission current is controlled with an additional electrode. Such a scheme providing a lowered level of power consumption has been realized in the recent publication [159]. In this work, single-walled nanotubes were produced by the standard electric arc method in a helium atmosphere. 1 g of the initial soot containing 60 wt .% single-walled CNTs was stirred for several minutes in 200 ml of concentrated sulfuric/nitric acid solution of varied composition. Then the suspension obtained was stirred for several hours at 100–120 °C and filtered by means of a polytetrafluoroethylene filter paper. The filtered wet powder was washed with distilled water several times and dried at room temperature, thereafter it was flooded again with distilled water and ultrasonicated. In order to get a surface charge on the nanotube powder, from 10^{-6} to 10^{-2} mol of $Mg(NO_3)_2 \cdot 6H_2O$ was added to the powder suspension. The electrophoresis coating method was used to deposit carbon nanotubes onto a patterned metal cathode. In accordance with the former, a negative dc bias of 10–50 V was applied to the cathode, which resulted in selective deposition of nanotubes on the patterned electrode surface. As follows from SEM and TEM observations, Raman spectral measurements and thermogravimetry analysis, the nanotubes obtained are bound into bundles of 10–30 nm in diameter and do not contain metal contaminants.

As is stated through numerical calculations, the electric field amplification effect strongly disturbs the homogeneity of the electron emission current over the edge surface of a bundle, so that the current density emitted from a periphery site of the surface considerably exceeds that for a middle region. In order to avoid this phenomenon, a gate electrode was incorporated between cathode and anode, which results in a triode structure for an element of the panel. The gate electrode has a set of holes of 300 μm in diameter, providing the passage of emitted electrons, and is separated by 1100 μm from the anode. A green-light-emitting phosphor ZnS : Cu, Al was utilized for characterization of the field emission. The gate bias was ranged between 100 and 300 V with a sine pulse of frequency 25 kHz. The brightness of the panel luminescence is determined by the anode voltage. Thus, a brightness of 1000 cd m^{-2} was achieved at a voltage of 220 V on the gate, and 900 V on the anode. The image on the screen is characterized by a high degree of surface homogeneity and time stability. The fluctuation level of the brightness at a pressure of 5×10^{-6} Torr in the chamber did not exceed 5% over 12 h.

Cathode ray tube lighting lamps and screens. The high emission properties of CNT-based cathodes open up possibilities for their use not only in flat panel displays but in other electron beam devices as well. One such a device is the cathode ray tube lighting lamp, where a phosphor layer irradiated with an electron beam is utilized as a source of light. Hot cathodes possessing quite high emission characteristics are in common use for this purpose. However, the necessity of heating the electron beam source up to several hundred

degrees Celsius complicates the design of the lamp and enhances the energy consumption. A construction containing an electron field emitter with CNT-based cathode is almost devoid of these disadvantages. This construction has been described, in particular, in work [160], where the possibility of effective application of a cathode based on multiwalled nanotubes to lighting sources has been demonstrated and the operation of a CNT-based electron emitter has been performed for 10,000 h.

Multiwalled nanotubes were produced by the standard electric arc method at a He pressure of 200 – 500 Torr, discharge current of 50 – 70 A and a voltage of about 25 V. The anode was 6 mm in diameter, and the cathode was 13 mm in diameter. The material containing nanotubes in the form of a disk 0.5 – 1 mm in thickness and 6 mm in diameter was extracted out of the inner part of the cathode deposit and was glued to a stainless steel plate ($5 \times 5 \times 0.15$ mm) using silver paste. After annealing in air at 450 – 500 °C, the hard outer shells of the deposit were removed, leaving on the disc surface only a nanotube-containing fibrous core 2 – 3 mm in diameter. The disc obtained was inserted into a cathode ray tube instead of a conventional hot cathode. The cathode electron emission was controlled by means of a grid electrode separated by 0.5 – 1 mm from the cathode. An aluminium film 100 – 150 nm in thickness, deposited onto a glass substrate and coated with a phosphor, was utilized as an anode. The device was pumped out down to a pressure of 10^{-8} Torr. The cathode was grounded and the control grid electrode voltage was varied between 0.6 and 1.2 kV. The anode voltage was typically 10 kV. As follows from experimental findings, approximately 60% of the emission current passes through the grid and reaches the anode. The emission current fluctuation level does not exceed 4% over 10 min. The measurements performed with emitters on the basis of individual CNTs and color phosphors (green ZnS : Cu, Al; red Y_2O_3 : Eu, and blue ZnS : Ag) implied that an anode current of 200 μA provided a luminescence brightness of 6.3×10^4, 2.3×10^4 and 1.5×10^4 cd m^{-2}, correspondingly. This is about twice of the relevant magnitude inherent to commercial thermal emission electron sources operating at a current of 100 μA. The parameters of the device described are quite high for its employment in giant outdoor displays.

A fascinating modification of a vacuum cathode ray light source with a CNT-based cathode was demonstrated in the recent work [161], where the cylindrical structure of the cathode was realized, as distinct from traditionally developed flat CNT-based sources. This structure is presented schematically in Fig. 20. A wire 1 mm in diameter and 7 cm in length, manufactured from Fe – Al – Cr alloy, was utilized as a substrate. It was coated with $Fe(NO_3)_3 \cdot 9H_2O$ solution containing iron acting as a catalyst. Nanotubes were grown on the surface of the substrate placed into a cylindrical quartz reactor 12 mm in diameter under a flow of acetylene (20 ml min^{-1}) and nitrogen (80 ml min^{-1}) at 720 °C and atmospheric pressure. As a result of the synthesis process, bent multiwalled CNTs of about 20 nm in diameter were grown on the cylindrical substrate surface. The emission properties of the cathode manufactured were studied using a cylindrical aluminium anode 21 mm in radius and 5 cm in length placed into a vacuum chamber of about 10^{-10} bar in pressure. The measured current – voltage characteristic of the emitter is in good agreement with the classic Fowler – Nordheim dependence over the voltage range below 500 V. The measurements indicated that an emission current density of 1 mA cm^{-2} was reached at the voltage of 1.1 kV, which is a record achievement for an interelectrode separation of about 2 cm. This result can be explained, in particular, by the cylindrical geometry of electrodes, providing a $\ln(r_2/r_1)$ increase of the electric field strength in proximity to the cathode in comparison with the case of flat geometry (r_1 is the cathode radius, r_2 is the anode radius). Processing the current – voltage characteristics of the emitter based on the Fowler – Nordheim expression (5) and assuming the electron work function of a nanotube to be close to 5 eV provides an estimate of the electric field amplification factor of CNTs, which turned out to be 23,000.

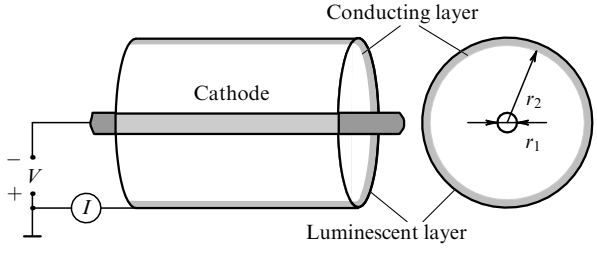

Figure 20. Schematic of a cylindrical cathode ray tube illuminating lamp with a CNT-based cathode [161]. The cylinder is 5 cm in length and 2.1 cm in radius (r_2).

The emitter manufactured has been utilized as a cathode for a luminescent lighting lamp. A cylindrical glass tube, the inner surface of which was coated with a phosphor, was utilized as an anode. The cathode emission current density reached 0.5 mA cm^{-2} at an applied voltage of 5.4 kV, which corresponds to an anode current density of 0.06 mA cm^{-2}. In this case the luminescence reached 10,000 cd m^{-2}, which is comparable to that of commercial luminescent lamps. However, in contrast to conventional luminescent lighting lamps, the above-described source does not contain ecologically dangerous mercury, and is easily ignited and quenched.

X-ray sources. CNT-based cathodes have been successfully taken up as the electron emitter in an X-ray source [162]. In contrast to conventional thermal emission cathodes, such devices do not consume energy for heating the cathode, which promotes the design of compact portable facilities, and are not exposed to the chemical action of rest H_2O and O_2 molecules with the hot metal cathode surface, resulting in its damage. The experiments were performed in a vacuum chamber equipped with a beryllium window for passing X-rays at an electron beam current of 1.5 μA and a pressure of 2×10^{-7} Torr. Multiwalled nanotubes aligned perpendicularly to the surface were grown on the surface of a tungsten wire with a Co plating, which was used as an emitter. The surface density of the nanotubes was estimated as 6×10^7 mm^{-2}. The nanotube caps contained metal nanoparticles (Co). The electron beam current was controlled by changing the voltage applied to a counter-electrode. Provision was made for the possible replacement of the CNT-based cathode with a standard thermal emission cathode.

A large-scale integrated circuit was used as the first object of investigations. The characteristic magnitude of the electron beam energy was 60 kV. An X-ray photograph of the object contains a clearly discriminable image of gold wires 30 μm in diameter. Comparison of images of the integrated circuit, obtained with the CNT-based and thermal emission cathodes, points to the significantly higher quality of the CNT-

produced image. Some details of the circuit are visible only using the X-ray tube with the CNT-based cathode but remain indistinguishable in the case of a thermal emission cathode. A leaf of a living tree was employed as the second object of investigations. The X-ray image of it promoted a conclusion about the nutrition transportation through the leaf veins. The measurements were performed at a beam energy of 10 keV and an exposure time of 1 h. The attained quality of the X-ray image of the leaf is unachievable using a conventional device with a thermal emission cathode. Thus, X-ray tubes equipped with CNT-based cathodes have none of the disadvantages inherent to thermal emission cathodes and provide a higher quality of the object image.

Cathodes of gas discharge devices. The high emission properties of CNTs are attractive not only for the development of cathodes for high-vacuum devices, but also for gas discharge setups. These cathodes are distinguished by a relatively low breakdown voltage, which follows from the low threshold of the electron field emission. However, in the operating conditions of a gas discharge device the cathode surface is persistently subject to ion irradiation, which results in the rapid damage of nanotubes and lowers the emission characteristics of the cathode. Therefore, CNT-based cathodes can be used in gas discharge devices only in conditions of short operation period. Such conditions occur, in particular, in gas discharge facilities protecting electrical circuits from extra voltage. A device of a similar kind has been designed and tested by Rosen et al. [163]. This is a tube filled with an inert gas which does not conduct electric current under normal voltage. Under a large transient voltage, such as from lightning, breakdown occurs, and the current of this device protects the circuit which is subjected to an extra voltage. The main disadvantages of conventional gas discharge protectors relate to the rather low reproducibility of the breakdown voltage and also to the slow response for a sudden change in sign of the extra voltage. Besides, due to the relatively high breakdown voltage these devices have to work at a low interelectrode gap, the breakdown voltage turning out to be very sensitive to the width of the gap.

The above-mentioned problems can be resolved using a cathode on the basis of single-walled nanotubes. Nanotubes of 1.4 nm in average diameter, bound into bundles of 15–30 nm in diameter, were produced through the laser ablation method. The soot was first purified in flowing 20% H_2O_2 at 100 °C, which was followed by the filtration in methanol and ultrasonication. After drying in a vacuum the material was studied by means of TEM and an X-ray diffractometer. These studies demonstrated that the material contained 80–90% of single-walled nanotubes and a handful of admixed particles of Ni and Co, and also graphite nanoparticles. Molybdenum discs 18 mm in diameter, coated with a thin (50 μm) layer of Pt, Al or Fe, have been used as cathodes of the gas discharge devices. The Pt layer was applied using the ion deposition method, whereas the Al and Fe layers were applied through the thermal vaporization method. A film of purified nanotubes was deposited on the substrate prepared in the above-described manner. Some electrode samples were annealed for 0.5 h at a pressure of 5×10^{-6} Torr and temperatures of 650 °C (Al), 850 °C (Fe) and 1150 °C (Pt).

The emission properties of the cathode were studied in the parallel plate geometry with an interelectrode separation of 500 μm and 10^{-6}-Torr vacuum, and also on filling the gap with various buffer gases. As an anode, a plain Mo plate was utilized. In the case of the bipolar gas discharge device the anode and cathode were similar to each other, and the interelectrode separation was kept at the level of 1 mm by means of special fixators. The breakdown voltage was evaluated on the basis of 1000 tests. The emission current–voltage characteristics measured for cathodes with various substrates are in agreement with the Fowler–Nordheim dependence, which implies a field emission origin of the current. The onset voltage for the emission current of 1 μA was equal to 600 V (electric field strength of 1.2 V μm^{-1}) for the annealed CNT/Fe/Mo and CNT/Al/Mo cathodes; 660 V (1.3 V μm^{-1}) for the unannealed CNT/Fe/Mo cathode, and 1260 V (2.5 V μm^{-1}) for the annealed CNT/Pt/Mo cathode. For the above-listed set of cathodes, the magnitude of the field intensity providing a current density of 1 mA cm^{-2} was equal to 1.7, 2.3, 2 and 3 V μm^{-1}, correspondingly. The observed distinction between emission characteristics of cathodes differing in the substrate material can be explained by the difference in the quality of the electrical contact between the metal and CNT. A strong dependence of the breakdown voltage on the pressure and sort of the buffer gas has been found. For instance, in the case of the annealed CNT/Fe/Mo cathode and Ar as a buffer gas the most reliable breakdown data relate to the Ar pressure of 0.5 Torr. A further increase in the Ar pressure is accompanied by a lowering in the breakdown voltage and also in the degree of repeatability of the data. The comparison of breakdown characteristics of the above-described gas discharge device with those of commercial analogues operating at the same interelectrode separation (1 mm) indicates that using CNTs as an emitter lowers the breakdown voltage by approximately 25% (to 450 V), and the root-mean-square deviation of this parameter by a factor of 4–20. A rise in the number of breakdowns causes a weak lowering in the breakdown voltage, which reaches a magnitude of 400 V after 1000 breakdown trials.

7. Conclusions

The discovery of the carbon nanotubes is one of the most considerable achievements of the modern science. This carbon modification is intermediate in its structure between graphite and fullerenes. However, carbon nanotubes in respect to many properties have nothing to do with either graphite or fullerenes. This permits one to consider and study nanotubes as a proper material possessing unique physical and chemical characteristics.

Carbon nanotubes, like fullerenes, have been discovered in a course of purely basic research focused on establishing the origin and structural characteristics of carbon clusters formed as a result of the thermal decomposition of graphite. However, shortly after the discovery of nanotubes it was found that their unique physical and chemical properties offer scope for a great variety of applications. In particular, their good electrical conduction in combination with tiny size make nanotubes a unique source of the electron field emission. The use of nanotubes as electron field emitters in cold cathodes permits one to improve significantly the operating characteristics of such devices as flat panel displays, cathode ray tube illuminating lamps, X-ray tubes, etc. Electronic devices with a CNT-based cathode are distinguished by their high degree of time stability, reduced overall dimension and weight and also reduced level of energy consumption. Therefore, one can expect that such devices, whose first prototypes have been developed and tested over the last 2–3 years, will become widespread in the near future.

Researchers working in the field of carbon nanotubes have travelled a considerable way during the 10 years which have passed from their discovery. The following issues can be noted as important stages characterizing this way: the discovery of multiwalled [7] and, subsequently, single-walled [36] nanotubes; the discovery of the capillary phenomena and ability to fill nanotubes with liquid substances [27]; the establishment of an interconnection between the structural and electronic characteristics of a single-walled nanotube [105]; the elaboration of the method for production of CNTs on the basis of thermal catalytic decomposition of hydrocarbons [164]; the discovery of the electron field emission from nanotubes [24, 25]; the elaboration of a method for the production of nanotubes with close structural and electronic characteristics [37]; the development of methods for homogeneous filling of large patterned surfaces with similarly aligned nanotubes having close electronic characteristics [34], and the manufacture of a model sample of a flat panel display with a CNT-based cold cathode [26]. The above-presented list of achievements in the field is easy to continue; however, it is already obvious that during a short time period we have seen a transition from the description of elongated objects forming as a result of thermal decomposition of graphite through synthesis of nanotubes with pregiven structural and electronic characteristics to the fabrication of reliably operating devices with CNT-based cathodes. This example shows once again the important fruitful role of basic research which can result in the quick progress of applied technology for a successful concurrence of circumstances.

The solution to the problem of the application of CNTs depends primarily on the production cost of nanotubes in a macroscopic amount. As of now, it considerably exceeds that of gold, which apparently excludes the possibility of large-scale application of this material. Nevertheless, such properties of nanotubes as their extra tiny size, good electrical conduction, high emission characteristics, etc. allow one to hope for their effective application in such fields as measuring techniques, electronics and nanoelectronics, chemical technology and so forth. The successful solution of these problems will become one more example of the effective influence of basic research on scientific and technological progress.

References

1. Kroto H W et al. *Nature* **318** 162 (1985)
2. Kratschmer W et al. *Nature* **347** 354 (1990)
3. Eletskiĭ A V, Smirnov B M *Usp. Fiz. Nauk* **163** (2) 33 (1993) [*Sov. Phys. Usp.* **36** 202 (1993)]; **165** 977 (1995) [*Phys. Usp.* **38** 935 (1995)]
4. Smalley R E *Rev. Mod. Phys.* **69** 723 (1997); *Usp. Fiz. Nauk* **168** 323 (1998)
5. Curl R F *Rev. Mod. Phys.* **69** 691 (1997); *Usp. Fiz. Nauk* **168** 331 (1998)
6. Kroto H *Rev. Mod. Phys.* **69** 703 (1997); *Usp. Fiz. Nauk* **168** 343 (1998)
7. Iijima S *Nature* **354** 56 (1991)
8. Eletskiĭ A V *Usp. Fiz. Nauk* **167** 945 (1997) [*Phys. Usp.* **40** 899 (1997)]
9. Kasumov A Yu et al. *Science* **284** 1508 (1999)
10. Morpurgo A F et al. *Science* **286** 263 (1999)
11. Bandow S et al. *Phys. Rev. Lett.* **80** 3779 (1998)
12. Guo T et al. *J. Phys. Chem.* **99** 10694 (1995); *Chem. Phys. Lett.* **243** 49 (1995); Rinzler A G et al. *Appl. Phys. A* **67** 29 (1998)
13. Laplaze D et al. *C.R. Acad. Sci.* **318** 733 (1994)
14. Yacamàn M J et al. *Appl. Phys. Lett.* **62** 202 (1993)
15. Bower C et al. *Appl. Phys. Lett.* **77** 2767 (2000)
16. Hsu W K et al. *Nature* **377** 687 (1995); *Chem. Phys. Lett.* **262** 161 (1996)
17. Cho W-S et al. *Appl. Phys. Lett.* **69** 278 (1996)
18. Li Y L, Yu Y D, Liang Y *J. Mater. Res.* **12** 1678 (1997)
19. Peigney A et al. *J. Mater. Res.* **12** 613 (1997)
20. Diener M D, Nichelson N, Alford J M *J. Phys. Chem. B* **104** 9615 (2000)
21. Dresselhaus M S, Dresselhaus G, Eklund P C *Science of Fullerenes and Carbon Nanotubes* (San Diego: Academic Press, 1996)
22. Saito R, Dresselhaus G, Dresselhaus M S *Physical Properties of Carbon Nanotubes* (London: World Scientific Publ., 1998)
23. Ebbesen T W *Carbon Nanotubes: Preparation and Properties* (Boca Raton, Fl.: CRC Press, 1997)
24. Gulyaev Yu V et al. *Le Vide Les Chouches Minces* (Suppl. 271) 322 (1994); in *7th Intern. Vacuum Microelectronics Conf., July 1994, France*; *J. Vac. Sci. Technol. B* **13** 435 (1995); Chernozatonskii L A et al., in *MRS Fall Meeting 1994, Boston, Mass., USA* (1994) p. 271; *Chem. Phys. Lett.* **233** 63 (1995); in *8th Intern. Vacuum Microelectronics Conf., July 1995, Portland, Oregon*, Tech. Digest (1995) p. 363; *J. Vac. Sci. Technol. B* **14** 2080 (1996); Sinitsyn N I et al. *Appl. Surf. Sci.* **111** 145 (1997)
25. De Heer W A, Châtelain A, Ugarte D *Science* **270** 1179 (1995)
26. Wang Q H et al. *Appl. Phys. Lett.* **72** 2912 (1998); Saito Y, Uemura S, Hamaguchi K *Jpn. J. Appl. Phys. Pt. 2* **37** L346 (1998)
27. Ajayan P M, Iijima S *Nature* **361** 333 (1993)
28. Dillon A C et al. *Nature* **386** 377 (1997)
29. Salvetat J-P et al. *Appl. Phys. A* **69** 255 (1999)
30. Akita S et al. *J. Phys. D* **32** 1044 (1999)
31. Calvert P *Nature* **399** 210 (1999)
32. Reulet B et al. *Phys. Rev. Lett.* **85** 2829 (2000)
33. Grobert N et al., in *Electronic Properties of Novel Materials — Progress in Molecular Nanostructures: XII Intern. Winterschool, Austria, March 1998* (AIP Conf. Proc., Vol. 442, Eds H Kuzmany et al.) (Woodbury, N.Y.: AIP, 1998) p. 29
34. Ren Z F et al. *Science* **282** 1105 (1998); Fan S et al. *Science* **283** 512 (1999); see also Ref. [87]; Li J et al. *Appl. Phys. Lett.* **75** 367 (1999)
35. Hamada N, Sawada S, Oshiyama A *Phys. Rev. Lett.* **68** 1579 (1992)
36. Iijima S, Ichihashi T *Nature* **363** 603 (1993)
37. Thess A et al. *Science* **273** 483 (1996)
38. Journet C et al. *Nature* **388** 756 (1997)
39. Lamy de la Chapelle M et al. *Carbon* **36** 705 (1998)
40. Journet C, Bernier P *Appl. Phys. A* **67** 1 (1998)
41. Cowley J M et al. *Chem. Phys. Lett.* **265** 279 (1997)
42. Henrard L et al. *Eur. Phys. J. B* **13** 661 (2000)
43. Bernaerts D et al. *Solid State Commun.* **105** 145 (1998)
44. Qin L C et al. *Chem. Phys. Lett.* **268** 101 (1997)
45. Venema L C et al. *Phys. Rev. B* **61** 2991 (2000)
46. Rao A M et al. *Science* **275** 187 (1997)
47. Liu B et al. *Chem. Phys. Lett.* **320** 365 (2000)
48. Saito R et al. *Phys. Rev. B* **57** 4145 (1998)
49. Jost O et al. *Appl. Phys. Lett.* **75** 2217 (1999)
50. Kataura H et al. *Synth. Met.* **103** 2555 (1999)
51. Sawada S, Hamada N *Solid State Commun.* **83** 917 (1992)
52. Peng L-M et al. *Phys. Rev. Lett.* **85** 3249 (2000)
53. Sun L F et al. *Nature* **403** 384 (2000)
54. Qin L-C et al. *Nature* **408** 50 (2000)
55. Peng H Y et al. *Appl. Phys. Lett.* **77** 2831 (2000)
56. Wang N et al. *Nature* **408** 50 (2000)
57. Prinzbach H et al. *Nature* **407** 60 (2000)
58. Bernaerts D et al., in *Physics and Chemistry of Fullerenes and Derivatives: Proc. of the Intern. Winterschool on Electronic Properties of Novel Materials* (Eds H Kuzmany et al.) (Singapore: World Scientific, 1995) p. 551
59. Zettl A, Cummings J, in *Electronic Properties of Novel Materials — Molecular Nanostructures: XIV Intern. Winterschool / Euroconf., Austria, 2000* (AIP Conf. Proc., Vol. 544, Eds H Kuzmany et al.) (Melville, N.Y.: AIP, 2000) p. 526
60. Mordkovich V Z et al. *Carbon* **34** 1301 (1996)
61. Mordkovich V Z et al., in *New Horizons of π-Electron Materials* (Berlin: Springer-Verlag, 1997)
62. Yudasaka M et al. *Appl. Phys. Lett.* **67** 2477 (1995)
63. Ruoff R S et al. *Nature* **364** 514 (1993)
64. Zhou O et al. *Science* **263** 1744 (1994)
65. Liu M, Cowley J M *Carbon* **32** 393 (1994)
66. Liu M, Cowley J M *Ultramicroscopy* **53** 333 (1994)

67. Kosaka M et al. *Chem. Phys. Lett.* **233** 47 (1995)
68. Huira H et al. *Nature* **367** 148 (1994)
69. Bursill L A, Peng J-L, Fan X-D *Philos. Mag. A* **71** 1161 (1995)
70. Zhang X B et al. *Europhys. Lett.* **27** 141 (1994)
71. Ivanov V et al. *Chem. Phys. Lett.* **223** 329 (1994); *Carbon* **33** 1727 (1995)
72. Amelinckx S et al. *Science* **265** 635 (1994); Bernaerts D et al. *Philos. Mag. A* **71** 605 (1995)
73. Biró L P et al. *Phys. Rev. B* **56** 12490 (1997); *Appl. Phys. Lett.* **73** 3680 (1998)
74. Weldon D N, Blau W J, Zandlbergen H W *Chem. Phys. Lett.* **241** 365 (1995)
75. Ishigami M et al. *Chem. Phys. Lett.* **319** 457 (2000)
76. Ando Y et al. *Chem. Phys. Lett.* **323** 580 (2000)
77. Dillon A C et al. *Chem. Phys. Lett.* **316** 13 (2000)
78. Zhang Y, Gu H, Iijima S *Appl. Phys. Lett.* **73** 3827 (1998)
79. Journet C et al. *Synth. Met.* **103** 2488 (1999)
80. Walker P L (Jr), Rakszawski J F, Imperial G R *J. Phys. Chem.* **63** 133 (1969)
81. Ruston W R et al. *Carbon* **7** 47 (1969)
82. Robertson D *Carbon* **8** 365 (1970)
83. Baird T, Frayer J R, Grant B *Nature* **253** 329 (1969)
84. Song X Y et al. *J. Mater. Res.* **10** 251 (1994)
85. Rodriguez N M, Kim M S, Baker R T K *J. Phys. Chem.* **98** 13108 (1994)
86. Li W Z et al. *Science* **274** 1701 (1996)
87. Suh J S, Lee J S *Appl. Phys. Lett.* **75** 2047 (1999)
88. Sung S L et al. *Appl. Phys. Lett.* **74** 197 (1999)
89. Tang Z K et al. *Appl. Phys. Lett.* **73** 2287 (1998)
90. Xie S S et al. *Adv. Mater.* **11** 1135 (1999)
91. Biró L P et al. *Appl. Phys. Lett.* **76** 706 (2000)
92. Rohmund F, Falk L K L, Campbell E E B, in *Electronic Properties of Novel Materials — Molecular Nanostructures: XIV Intern. Winterschool / Euroconf., Austria, 2000* (AIP Conf. Proc., Vol. 544, Eds H Kuzmany et al.) (Melville, N.Y.: AIP, 2000) p. 234; *Chem. Phys. Lett.* **328** 369 (2000); Bladh K, Falk L K L, Rohmund F *Appl. Phys. A* **70** 317 (2000)
93. Fan S et al. *Physica E* **8** 179 (2000)
94. Colomer J-F et al. *Chem. Commun.* (14) 1343 (1999); Willems I et al., in *Electronic Properties of Novel Materials — Molecular Nanostructures: XIV Intern. Winterschool / Euroconf., Austria, 2000* (AIP Conf. Proc., Vol. 544, Eds H Kuzmany et al.) (Melville, N.Y.: AIP, 2000) p. 242
95. Fischer J E et al., in *Electronic Properties of Novel Materials — Progress in Molecular Nanostructures: XII Intern. Winterschool, Austria, 1998* (AIP Conf. Proc., Vol. 442, Eds H Kuzmany et al.) (Woodbury, N.Y.: AIP, 1998) p. 34
96. Bezmel'nitsyn V N, Eletskiĭ A V, Okun' M V *Usp. Fiz. Nauk* **168** 1195 (1998) [*Phys. Usp.* **41** 1091 (1998)]
97. Eletskiĭ A V *Usp. Fiz. Nauk* **170** 113 (2000) [*Phys. Usp.* **43** 111 (2000)]
98. Duesberg G S et al., in *Electronic Properties of Novel Materials — Progress in Molecular Nanostructures: XII Intern. Winterschool, Austria, 1998* (AIP Conf. Proc., Vol. 442, Eds H Kuzmany et al.) (Woodbury, N.Y.: AIP, 1998) p. 39
99. Holzinger M et al., in *Electronic Properties of Novel Materials — Molecular Nanostructures: XIV Intern. Winterschool / Euroconf., Austria, 2000* (AIP Conf. Proc., Vol. 544, Eds H Kuzmany et al.) (Melville, N.Y.: AIP, 2000) p. 246
100. Holzinger M et al. *Appl. Phys. A* **70** 599 (2000)
101. Bougrine A et al. *Synth. Met.* **103** 2480 (1999)
102. Shi Z et al. *Solid State Commun.* **112** 35 (1999)
103. Mizoguti E et al. *Chem. Phys. Lett.* **321** 297 (2000)
104. Zhang M et al. *Chem. Phys. Lett.* **328** 350 (2000)
105. Saito R et al. *Appl. Phys. Lett.* **60** 2204 (1992)
106. Charlier J-C, Michenaud J-P *Phys. Rev. Lett.* **70** 1858 (1993)
107. Maarouf A A, Kane C L, Mele E J *Phys. Rev. B* **61** 11156 (2000)
108. White C T, Robertson D H, Mintmire J W *Phys. Rev. B* **47** 5485 (1993)
109. Mintmire J W et al. *Mater. Res. Soc. Symp. Proc.* **247** 339 (1992)
110. Mintmire J W, Dunlap B I, White C T *Phys. Rev. Lett.* **68** 631 (1992)
111. Tanaka K et al. *Chem. Phys. Lett.* **191** 469 (1992)
112. Harigaya K *Phys. Rev. B* **45** 12071 (1992)
113. Odom T W et al. *Nature* **391** 62 (1998)
114. Odom T W et al. *J. Mater. Res.* **13** 2380 (1998)
115. Odom T W et al. *J. Phys. Chem. B* **104** 2794 (2000)
116. Yorikawa H, Muramatsu S *Phys. Rev. B* **50** 12203 (1994)
117. Postma H W Ch et al. *Phys. Rev. B* **62** R10653 (2000)
118. Bachtold A et al. *Nature* **397** 673 (1999); *Phys. Rev. Lett.* **84** 6082 (2000)
119. Schönenberger C et al. *Appl. Phys. A* **69** 283 (1999)
120. Dai H, Wong E W, Lieber C M *Science* **272** 523 (1996)
121. Kong J et al. *Appl. Phys. A* **69** 305 (1999)
122. Krstic V et al., in *Electronic Properties of Novel Materials — Molecular Nanostructures: XIV Intern. Winterschool / Euroconf., Austria, 2000* (AIP Conf. Proc., Vol. 544, Eds H Kuzmany et al.) (Melville, N.Y.: AIP, 2000) p. 367
123. Frank S et al. *Science* **280** 1744 (1998)
124. Collins P G et al., in *Electronic Properties of Novel Materials — Molecular Nanostructures: XIV Intern. Winterschool / Euroconf., Austria, 2000* (AIP Conf. Proc., Vol. 544, Eds H Kuzmany et al.) (Melville, N.Y.: AIP, 2000) p. 385
125. Gomer R *Field Emission and Field Ionization* 2nd ed. (New York: AIP, 1993)
126. Hawkes P W, Kasper E "Theory of electron emission", in *Principles of Electron Optics* Vol. 2 *Applied Geometrical Optics* (London: Academic Press, 1989) Ch. 44
127. Landau L D, Lifshitz E M *Elektrodinamika Sploshnykh Sred* (Electrodynamics of Continuous Media) (Moscow: GITTL, 1957) [Translated into English (Oxford: Pergamon Press, 1960)]
128. Fransen M J, van Rooy Th L, Kruit P *Appl. Surf. Sci.* **146** 312 (1999)
129. Kai J et al. *Jpn. J. Appl. Phys. Pt. 1* **40** 4696 (2001)
130. Saito Y et al. *Jpn. J. Appl. Phys. Pt. 2* **36** L1340 (1997)
131. Stratton R *Phys. Rev.* **125** 67 (1962)
132. Stratton R *Phys. Rev.* **135** A794 (1964)
133. Venema L C et al. *Phys. Rev. B* **61** 2991 (2000)
134. Jorio A et al. *Phys. Rev. Lett.* **86** 1118 (2001)
135. Chen Y, Shaw D T, Guo L *Appl. Phys. Lett.* **76** 2469 (2000)
136. Collins P G, Zettl A *Phys. Rev. B* **55** 9391 (1997)
137. Küttel O M *Appl. Phys. Lett.* **73** 2113 (1998)
138. Bonard J-M et al. *Appl. Phys. Lett.* **73** 918 (1998)
139. Nilsson L et al. *Appl. Phys. Lett.* **76** 2071 (2000)
140. Dean K A, Chalamala B R *Appl. Phys. Lett.* **76** 375 (2000)
141. Dean K A, von Allmen P, Chalamala B R *J. Vac. Sci. Technol. B* **17** 1959 (1999)
142. Dean K A, Chalamala B R *J. Appl. Phys.* **85** 3832 (1999)
143. Colazzo R, Schlesser R, Sitar Z *Appl. Phys. Lett.* **78** 2058 (2001)
144. Liu X et al., in *Electronic Properties of Novel Materials — Molecular Nanostructures: XIV Intern. Winterschool / Euroconf., Austria, 2000* (AIP Conf. Proc., Vol. 544, Eds H Kuzmany et al.) (Melville, N.Y.: AIP, 2000) p. 288
145. Suzuki S et al. *Appl. Phys. Lett.* **76** 4007 (2000)
146. Chen P et al. *Phys. Rev. Lett.* **82** 2548 (1999)
147. Ago H et al. *J. Phys. Chem. B* **103** 8116 (1999)
148. Shiraishi M, Hinokuma K, Ata M, in *Electronic Properties of Novel Materials — Molecular Nanostructures: XIV Intern. Winterschool / Euroconf., Austria, 2000* (AIP Conf. Proc., Vol. 544, Eds H Kuzmany et al.) (Melville, N.Y.: AIP, 2000) p. 359
149. Obraztsov A N, Volkov A P, Pavlovskiĭ I Yu *Pis'ma Zh. Eksp. Teor. Fiz.* **68** 56 (1998) [*JETP Lett.* **68** 59 (1998)]
150. Obraztsov A N et al. *Pis'ma Zh. Eksp. Teor. Fiz.* **69** 381 (1999) [*JETP Lett.* **69** 411 (1999)]
151. Obraztsov A N, Volkov A P, Pavlovsky I *Diamond Relat. Mater.* **9** 1190 (2000)
152. Obraztsov A N et al. *Diamond Relat. Mater.* **8** 814 (1999)
153. Obraztsov A N et al. *J. Vac. Sci. Technol. B* **18** 1059 (2000)
154. Obraztsov A N, Pavlovsky I Yu, Volkov A P *J. Vac. Sci. Technol. B* **17** 674 (1999)
155. Jeong S-H et al. *Appl. Phys. Lett.* **78** 2052 (2001)
156. Yamamoto K, Akita S, Nakayama Y *J. Phys. D* **31** L34 (1998)
157. Wang Q H et al. *Appl. Phys. Lett.* **72** 2912 (1998)
158. Choi W B et al. *Jpn. J. Appl. Phys. Pt. 1* **39** 2560 (2000)
159. Choi W B et al. *Appl. Phys. Lett.* **78** 1547 (2001)
160. Saito Y, Uemura S, Hamaguchi K *Jpn. J. Appl. Phys. Pt. 2* **37** L346 (1998)
161. Bonard J-M et al. *Appl. Phys. Lett.* **78** 2775 (2001)
162. Sugie H et al. *Appl. Phys. Lett.* **78** 2578 (2001)

163. Rosen R et al. *Appl. Phys. Lett.* **76** 1668 (2000)
164. José-Yacamán M et al. *Appl. Phys. Lett.* **62** 657 (1993)